Mapping the Proximal Proteome of the Recycling Endosomal Alkali Cation/Proton Exchanger NHE6/SLC9A6

Anthony Strina

Department of Physiology

McGill University

Montreal, Quebec, Canada

August 2023

A thesis submitted to McGill University in partial fulfillment of the requirements of the degree of Master of Science

TABLE OF CONTENTS

ABSTRACT

Recent genetic studies have linked mutations in *SLC9A6* to Christianson Syndrome (CS), a rare but increasingly diagnosed genetic disorder characterized by moderate to severe intellectual disability, epilepsy, ataxia, autistic behavior and neurodegeneration. This gene encodes for the alkali cation/proton exchanger NHE6 isoform that is expressed ubiquitously but is especially abundant throughout the central nervous system. Currently, the factors that govern the regulation and actions of NHE6 in neurons are poorly understood and treatment options are limited. Recent work by us and others has shown that NHE6 plays a major role in the trafficking and pH homeostasis of early and recycling endosomes, small intracellular membrane vesicles that carry proteins vital for neuronal growth and proper synaptic transmission. The loss of NHE6 causes excessive acidification of these vesicles as well as increased degradation of neurotrophic (e.g., TrkB receptor) and ionotropic (e.g., AMPA receptors) cargo – changes that are thought to underlie some of the neurological deficits associated with CS. To gain further mechanistic insight into the factors that govern the trafficking and regulation of NHE6, we have adopted a biotin-based protein-proximity labeling approach and applied it to the SH-SY5Y neuroblastoma cell line. This method uses a modified promiscuous biotin ligase derived from soybean ascorbate peroxidase (APEX2). The ligase is fused to a protein of interest (i.e., NHE6). Upon expression in cells, the NHE6-APEX2 chimera can be induced to biotinylate interacting and proximate proteins, which are identified via mass spectrometry. One of the interacting proteins identified from this method was Ras-related C3 botulinum toxin substrate 1, or RAC1, a Rho-GTPase involved in neurogenesis and cytoskeletal remodelling. Subsequent *in vitro* experiments, including co-immunoprecipitations, GST pull-downs and cell-surface biotinylation studies were performed to confirm the detected interaction between NHE6 and RAC1, as well as to examine its potential

biological significance. Results from my project indicate that wild-type RAC1 co-immunoprecipitates with NHE6 *in vitro* and binds to NHE6's C-terminus between amino acids 558-596. Moreover, a constitutively active RAC1 mutant forms a stronger co-immunoprecipitation complex with NHE6, thus indicating NHE6's importance in RAC1's signalling cascade when RAC1 is in an active state. Cell surface biotinylation experimentation revealed that RAC1 expression is more evident in the presence of NHE6 and exhibits a higher degree of localization to the cell's membrane. In conclusion, we propose that NHE6 plays an important role in RAC1's signalling cascade of cytoskeletal dynamics and cell re-modelling, factors important for neurogenesis.

ABRÉGÉ

Des études génétiques récentes ont lié des mutations du gène *SLC9A6* au syndrome de Christianson (SC), une maladie génétique rare mais de plus en plus diagnostiquée, caractérisée par une déficience intellectuelle modérée à sévère, l'épilepsie, l'ataxie, un comportement autistique et de la neurodégénérescence. Ce gène code pour l'isoforme NHE6 des échangeurs de cations alcalins/protons qui est exprimée de manière ubiquitaire mais qui est particulièrement abondante à travers le système nerveux central. Actuellement, les facteurs qui contrôlent la régulation et les actions de NHE6 dans les neurones sont mal compris et les options de traitement sont limitées. Des travaux récents de notre part et d'autres équipes de recherche ont montré que NHE6 joue un rôle majeur dans le trafic des protéines et l'homéostasie du pH des endosomes précoces et de recyclage, des petites vésicules membranaires intracellulaires, qui transportent des protéines vitales pour la croissance neuronale et pour la transmission synaptique. La perte de NHE6 provoque une acidification excessive de ces vésicules ainsi qu'une dégradation accrue de la cargaison neurotrophique (par exemple, le récepteur TrkB) et ionotrope (par exemple, les récepteurs AMPA) - des changements qui seraient à la base de certains des déficits neurologiques associés au SC. Pour mieux comprendre les mécanismes des facteurs qui contrôlent le trafic et la régulation de NHE6, nous avons adopté une approche de marquage de proximité des protéines à base de biotine et l'avons appliquée à la lignée cellulaire de neuroblastome SH-SY5Y. Cette méthode utilise une ligase de biotine avec une promiscuité modifiée dérivée de l'ascorbate peroxydase de soja (APEX2). La ligase est fusionnée à une protéine d'intérêt (c'est-à-dire, NHE6). Lors de l'expression dans les cellules, la chimère NHE6-APEX2 peut être induite pour ajouter des groupes de biotine aux protéines interagissant et proches, qui sont identifiées par la spectrométrie de masse. L'une des protéines en interaction

identifiées à partir de cette méthode était le substrat 1 de la toxine botulique C3 liée à Ras, ou RAC1, une Rho-GTPase impliquée dans la neurogenèse et le remodelage du cytosquelette. Des expériences *in vitro* ultérieures, notamment des co-immunoprécipitations, des pull-downs de GST et des études de biotinylation de la membrane cellulaire, ont été réalisées pour confirmer l'interaction détectée entre NHE6 et RAC1, ainsi que pour déterminer sa signification biologique potentielle. Les résultats de mon projet indiquent que RAC1 de type sauvage co-immunoprécipite avec NHE6 *in vitro* et se lie à l'extrémité C-terminale de NHE6 entre les acides aminés 558-596. De plus, un mutant de RAC1 de manière constitutivement actif forme un complexe de co-immunoprécipitation plus fort avec NHE6 et se lie à la même région sur l'extrémité C-terminale de NHE6, indiquant ainsi l'importance de NHE6 dans la cascade de signalisation de RAC1 lorsque RAC1 est en état actif. L'expérimentation de biotinylation de surface cellulaire a révélé que l'expression de RAC1 est plus évidente en présence de NHE6 et présente un degré de localisation plus élevé à la membrane cellulaire. En conclusion, nous proposons que NHE6 joue un rôle important dans la cascade de signalisation de RAC1 de la dynamique du cytosquelette et du remodelage cellulaire, des facteurs importants pour la neurogenèse.

CONTRIBUTION OF AUTHORS

Anthony Strina: Carried out most experiments, analyzed results and wrote the thesis.

Alina Ilie: Designed the NHE6$_{3F}$APEX2 and $_{F}$APEX2 constructs, designed the research project, and performed several experiments including APEX2 assay preparation for mass spectrometry identification, organellar pH measurements for proper NHE6 function, NHE6 and RAC1 co-localization studies and analyzed results.

John Orlowski: Designed and supervised the research project, analyzed mass spectrometry results, consulted for data interpretation, created BioRender figures and revised the thesis.

ACKNOWLEDGEMENTS

The achievement of completing my research project would not have been possible without the never-ending support of my supervisor, lab colleagues, friends, and family.

Firstly, I would like to express my sincere gratitude to my supervisor, Dr. John Orlowski. His invaluable contributions to the field of physiology, ground-breaking research and dedication have inspired countless individuals, including myself, to pursue a deeper understanding of the human body and its intricate workings. His passion for unravelling the complexities of physiology is evident in the numerous publications and studies he has authored, which have undoubtedly shaped the scientific community. I would like to personally thank him for the countless hours he has put into my project, whether it was interpreting the mass spectrometry data, correcting and reviewing my thesis and thesis proposal, professionalizing my words in a scientific manner and pushing me to always be meticulous. His contributions are a testament to his brilliance, and his legacy will continue to inspire future generations of physiologists.

Next, I would like to thank my lab colleagues Dr. Alina Ilie and Annie Boucher for their never-ending guidance and support throughout the past two years. Alina, the research associate, taught me mostly all the principles of all the experimental techniques I performed as well as how to interpret results. Although she was often busy taking care of her own experiments, she would always be happy to answer my many questions. Annie, the lab manager, was instrumental not only for me, but to the lab's proper coordination. She was always ready to solve any day-to-day issues or answer lab-related questions that arose. Most importantly, however, I thank Annie for her kindness and for creating such an enjoyable working environment, considering she was the closest lab member to my bench. I thank both Alina and Annie for the patience they showed towards my numerous lab mistakes and for helping me become a better researcher and co-worker.

I would next like to thank the other students in the Orlowski Lab during my presence there, Léo Han and Maëlle Bouchard Ouellet. They always did their best to contribute to positive vibes both inside and outside the lab. Léo also reviewed and did some of the spell-checking for this thesis. I would also like to thank the members of the CIS graduate body student body, notably Roy Shi and Shajenth Premachandran, who enriched my time here in the lab as a graduate student by providing helpful discussions on school- or outside-school-related topics.

I would also like to thank the members of my advisory committee, Dr. Gerhard Multhaup, Dr. Reza Sharif Naeini, and Dr. Anne McKinney, for their constructive feedback and for getting me to ask some of the bigger questions to better understand the overall picture of my project.

Finally, I would like to thank my mother and father, for supporting me during my master's research project. Their encouragement has played a significant role in my achievement. I am forever grateful for their belief in me for pursuing science.

LIST OF ABBREVIATIONS AND ACRONYMS

3F	Triple FLAG-tag
αMEM	alpha modification of Eagle's minimal essential medium
AAV	adeno-associated virus
Aβ	amyloid beta
ACACA	acetyl-CoA Carboxylase
ADHD	attention deficit hyperactivity disorder
AE2	anion exchanger 2
AMPA(-R)	α-amino-3-hydroxy-5-methyl-4-isoxazolepropionic acid (receptor)
AP-1	Chinese hamster ovary cell line containing negligible NHE6 levels
APEX2	ascorbate peroxidase 2
Arf6	ADP-ribosylation factor 6
Arp2/3	actin-related protein-2/3
AT2	Angiotensin II subtype receptor AT2
ATP	adenosine triphosphate
Aβ	amyloid beta
BDNF	brain-derived neurotrophic factor
β-tub	β-tubulin
BioID	proximity-dependent biotin identification
Ca^{2+}	calcium
CA	constitutively active
CALD1	caldesmon 1
CAMKII	Ca^{2+}/calmodulin-dependent protein kinase II
cAMP	cyclic adenosine monophosphate
CFL1	cofilin 1
CHO	Chinese hamster ovary
Cl^-	chlorine
ClC	family of chloride channels
CLTA	clathrin light chain A
CLTC	clathrin heavy chain
CNB	cyclic-nucleotide-binding
co-IP	co-immunoprecipitation
CPA	cation/proton antiporters
CS	Christianson syndrome
C-terminus	carboxy-terminus
CTTN	cortactin
D	aspartic acid
DAPI	4',6-diamidino-2-phenylindole
DN	dominant negative
DTT	dithiothreitol
dH_2O	distilled water
DMEM	Dulbecco's modified Eagle's minimum essential medium
DNA	deoxyribonucleic acid
DRG	dorsal root ganglion

DYNC1H1	dynein cytoplasmic 1 heavy chain 1
EDTA	ethylenediaminetetraacetic acid
EE	early endosome
F	FLAG-tag
F-actin	filamentous actin
GAP	GTPase activating protein
GEF	guanosine exchange factor
GFP	green fluorescent protein
GI	gastrointestinal
GST	glutathione-S-transferase
GPCR	G-protein coupled receptor
GTP	guanosine-5'-triphosphate
GO	gene ontology
H^+	proton
H	histidine
HA	influenza hemagglutinin peptide
HCO_3^-	bicarbonate
HGS	hepatocyte growth factor-regulated tyrosine kinase substrate
HRP	horseradish peroxidase
IPTG	isopropyl-β-D-thiogalactoside
JACoP	Just Another Colocalization Plugin
K^+	potassium
K	lysine
kDa	kilodalton
KEGG	Kyoto Encyclopedia of Genes and Genomes
KIF5B	kinesin I motor protein 5B
KO	knockout
L	leucine
LE	late endosomes
Li^+	lithium
LTP	long-term potentiation
MCC	Manders' colocalization coefficients
MCCC1	β-methylcrotonyl-CoA carboxylase
MVB	multi-vesicular bodies
mM	millimolar
mRNA	messenger ribonucleic acid
Mg^{2+}	magnesium
Mn^{2+}	manganese
MS	mass spectrometry
ms	millisecond (s)
N	asparagine
Na^+	sodium
NaCl	salt
$NaHCO_3$	sodium bicarbonate
NH_4^+	ammonium
NHE/NHA	sodium/proton exchanger or antiporter

nm	nanometer (s)
NMDA	N-methyl-D-aspartate
NTA	N-terminal acidic
OD	optical density
PAC	proton-activated Cl^- channel
PAK	p21-activated kinase 1
PBS	phosphate-buffered saline, pH 7.4
PC	pyruvate carboxylase
PCCA	propionyl-CoA-carboxylase
PCR	polymerase chain reaction
PFA	paraformaldehyde
pH	negative logarithm of the effective proton concentration
PM	plasma membrane
PPI	protein-protein interaction (s)
PVDF	polyvinylidene fluoride
Q	glutamine
R	arginine
RAC1	Ras-related C3 botulinum toxin substrate 1
RE	recycling
RhoGDI	Rho GDP-dissociation inhibitor
RIPA	radioimmunoprecipitation assay buffer
S	serine
SD	standard deviation
S.E.M.	standard error of the mean
SERCA	sarcoplasmic or endoplasmic reticulum Ca^{2+}-ATPases
SCAMP	secretory carrier membrane protein
SDS-PAGE	sodium dodecyl sulphate-polyacrylamide gel electrophoresis
SH-SY5Y	human neuroblastoma cell line
SLC	solute carrier gene family
SPCA	secretory pathway Ca^{2+}-ATPases
SPTBN1	spectrin β chain
T	threonine
TBS	tris-buffered saline
TCL	total cell lysates
Tf-A^{594}	Alexa Fluor ® 594-conjugated transferrin
Tf (R)	transferrin (receptor)
TGN	*trans*-Golgi network
TMEM165	transmembrane protein 165
Trk	tropomyosin receptor kinase
TRPV1	transient receptor potential cation channel subfamily V member 1
XLID	X-linked intellectual disability (ies)
V-ATPase	vacuolar-type proton ATPase pump
WT	wild type
YT	yeast exact tryptone
Zn^{2+}	zinc

LIST OF FIGURES AND TABLES

INTRODUCTION

1.1 Determinants of Organellar pH And Protein Trafficking

Eukaryotic cells segregate different biological processes within discrete organelles (i.e., nucleus, endoplasmic reticulum, Golgi apparatus, secretory vesicles, endosomes, lysosomes, peroxisomes and mitochondria) (1). The luminal ionic compositions of many, if not all, intracellular compartments differ from the surrounding cytoplasm and are important determinants of intracellular function (2). The establishment of these differential compositions is achieved through the concerted actions of distinct integral membrane ion carriers (2).

Organelles of the secretory and endocytic pathways are distinguished by their luminal acidity, with the $[H^+]$ varying by up to 100-fold between compartments (Fig. 1A) (3,4). Progressive acidification of organelles along the secretory pathway is important for proper post-translational processing, sorting, and transport of newly synthesized proteins (2,4,5). Likewise, graded acidification of vesicles along the endocytic pathway is essential for the recycling and/or degradation of internalized membrane proteins, fluid-phase solutes, and entry of various microbial organisms (4,6,7). Thus, fine control of organellar acidification is a fundamental cellular process; it is essential to understand the mechanisms that generate and regulate organellar pH homeostasis and its role in vesicular biogenesis and trafficking.

Acidification of endomembrane compartments involves an intricate balance between H^+ influx and efflux pathways, as well as counterion conductances (3,8). Active accumulation of H^+ in endomembrane compartments is largely achieved by a heterogeneous family of electrogenic vacuolar-type H^+-translocating ATP-hydrolases (V-ATPases) (3,5,9). These V-ATPases are assembled as multi-subunit complexes with a peripheral domain, V_1, which is responsible for converting the energy stored from ATP into the mechanical force necessary for H^+ displacement,

A

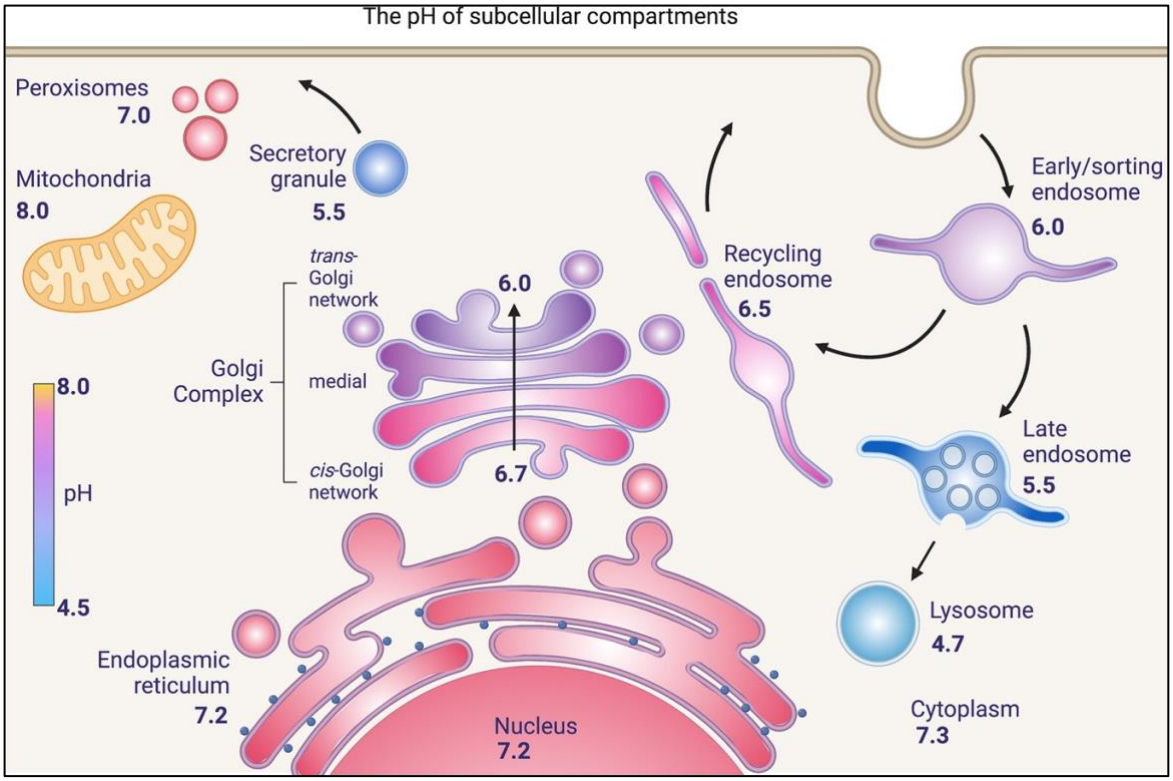

B

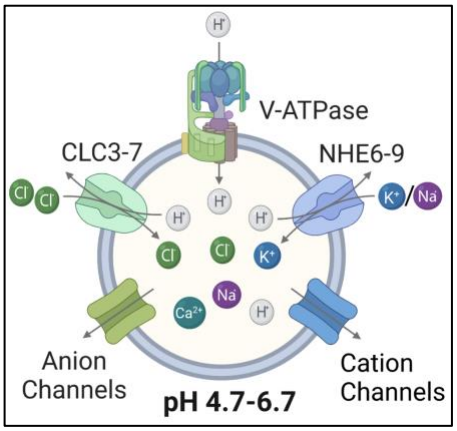

Figure 1 pH Homeostasis within the cell
(A) pH of the different subcellular compartments. Figure permission obtained from: *The American Physiological Society, 2023* (14). (B) Intraluminal channels are present for maintaining organellar pH. Image created with BioRender.

as well as a transmembrane domain, V_0, responsible for proton-translocation into the respective lumen (Fig. 1B) (4,9). Because V-ATPases translocate only H^+, an inner positive voltage is generated across the membrane, gradually impeding further influx of H^+. To facilitate greater acidification, parallel movement of counterions exist to neutralize the positive membrane potential (4,10). Channels or transporters mediating the entry of anions (e.g., Cl^-) or the efflux of cations (e.g., Na^+, K^+) have been identified as playing important roles in establishing the pH gradient among organelles (Fig. 1B). One of these includes electrogenic $2Cl^-/H^+$ exchangers of the chloride channel (ClC) transport family, sending Cl^- in and H^+ out of endomembrane lumens (11,12). Another recently discovered chloride-associated membrane protein that plays a role in conjunction with ClC exchangers is the proton-activated Cl^- (PAC) channel, which traffics from the plasma membrane to endosomes. Deletion of this channel elevates luminal Cl^- which generates a more acidic endosomal pH and enhances transferrin receptor-mediated endocytosis, a process reliant on endosomal pH (13). The efflux of cations, directing the outward movement of K^+, Na^+, Mg^{2+} and Ca^{2+}, has also been well established (14). Cation/proton antiporters (CPA), which are exchangers whose primary roles include regulating ion homeostasis for ions such as the movement of K^+, Na^+, Mg^{2+} and Ca^{2+}, also regulate pH as a secondary function (15). A subset of CPA are the mammalian alkali cation (Li^+, Na^+, K^+)/H^+ exchangers or antiporters, abbreviated as NHEs/NHAs, the focus of my project. A Ca^{2+}/H^+ antiport system present within vacuolar membrane vesicles of *Saccharomyces cerevisiae* has been proposed to play a potential role in organellar pH homeostasis on top of functioning primarily for calcium storage in mammals (17). Golgi cation homeostasis has been reported to be crucial for many cellular processes, including the glycosylation of proteins and vesicular fusions events (18). Notably, the transmembrane protein 165 (TMEM165) is responsible for Ca^{2+} and manganese (Mn^{2+}) transport in exchange for H^+ into the Golgi as a

regulator for the organ's acidity (18–21). Like the Golgi apparatus, other compartments require cation transporters, such as the sarcoplasmic or endoplasmic reticulum Ca^{2+}-ATPases (SERCAs) and secretory pathway (Golgi) Ca^{2+}-ATPases (SPCAs) (4). Different from V-ATPases, these pumps exchange protons for calcium and have been well-established as essential mechanisms for calcium delivery to organelles, having an indirect effect on organellar pH. Although not yet fully understood, ion exchangers propelling the influx of Mg^{2+} and possibly zinc (Zn^{2+}) for H^+ are also proposed to contribute to intraorganellar pH homeostasis, as this type of exchanger has been observed only in vacuolar membranes of *Arabidopsis thaliana* to date (22). Regulation of intraorganellar pH involves a precise balance between the many ion influx/efflux pathways and must be tightly regulated (4). These ions are present in the lumen of the endocytic and secretory pathways, and their involvement in pH homeostasis is being extensively studied.

1.1.1 Protein Trafficking Along the Endocytic Route

Endocytosis is responsible for the internalization of extracellular fluid, nutrients, receptor-ligand complexes, lipids, viruses, etc..., into nascent or primary endocytic vesicles that merge with early endosomes (EE) (23). Early endosomes are dynamic tubular-vesicular structures that serve as the initial sorting station for processing internalized material (23). Molecules present within these vesicles have different fates. Certain cargoes can be directed towards recycling endosomes (RE) where they can be rapidly transported back to the cell surface or towards the *trans*-Golgi network (TGN) for immediate reuse or storage for future deployment in response to various stimuli. Vesicles budding from EE can also mature to late endosomes (LE)/multivesicular bodies (MVB) which fuse with lysosomes to form an endolysosomal compartment where cargoes are degraded.

The process of how endocytic vesicles enter cells has been widely studied. Clathrin-mediated endocytosis is one of the most well-documented modes for the internalization of many proteins (24,25). Briefly, clathrin-coated pits, made up of a network of clathrin proteins arranged in a lattice-like pattern, are formed on the inner cell membrane following specific signalling events. As the pit forms, it starts to fold inward, gradually blebbing from the cell membrane until it is severed by a snipping protein, dynamin, forming a distinct separate vesicle known as a clathrin-coated vesicle. Clathrin proteins then dissociate and are recycled back to the cell membrane. The endocytosed vesicle, now free of clathrin, then fuses with EE.

Typically located at the periphery of the cell, EE have a unique structure with a central cell body ranging from ~100-500 nm in diameter with connected thin tubules of ~50 nm in diameter, while maintaining a slightly acidic environment (pH ~6.0) (26). As mentioned, their main function is to sort and organize molecules such as ligands or receptors, helping to determine their respective fates. It is the acidity within EE that allows many ligands to detach from their receptors, thus permitting the recycling of the latter to the plasma membrane (27). An example of this would be transferrin, the glycoprotein for mediating the transport of iron (28). Iron-bound transferrin (Tf) binds to the transferrin receptor (TfR) that is present on the cell membrane and subsequently undergoes internalization. Upon entry into the acidic environment of the EE, the iron dissociates from the ligand-receptor (Tf-TfR) complex (29). The Tf-TfR complex is then free to recycle/traffic back to the plasma membrane. Besides recycling, EE also play a role in directing molecules towards degradation, broadening its role in protein trafficking.

As mentioned above, the regulation of vesicular pH along the endocytic pathway is dynamic and an important factor in the processing, recycling, and degradation of internalized cargo. Intriguingly, it is also a critical determinant of vesicle trafficking, but the underlying mechanisms

are not well understood. One potential mechanism linking the regulation of pH to vesicle trafficking is V-ATPase's association with ADP-ribosylation factor 6 (Arf6), a known regulator of endocytosis. In the degradative endosomal pathway (i.e., early to late endosomes), Arf6 and its guanosine exchange factor (GEF) ARNO, interact directly with one of the V-ATPase isoforms in a manner dependent on luminal acidification, suggesting it functions not only as an acidification mechanism but also as a pH-sensor of the endosomal machinery for trafficking (30). This has led researchers to postulate that other endosomal pH-regulating transporters may also engage with the molecular machinery that controls vesicular trafficking events (4).

1.2 Alkali Cation/Proton Exchanger (SLC9) Gene Family

With over 450 members in the human genome, solute carriers (SLC) are only second to G-protein coupled receptors (GPCRs) which make up one of the largest gene families in vertebrates (31). The SLC9 gene family encodes for alkali cation (Li^+, Na^+, K^+)/proton (H^+) exchangers or antiporters (commonly referred to as Na^+/H^+ exchangers or antiporters, NHE or NHA, respectively). Thirteen different NHE/NHA genes (~13-71% protein similarity) are present in the mammalian genome and are sorted into three specific subfamilies: SLC9A-C (Fig. 2A) (32–34). These transporters are essential for many physiological processes, but are fundamentally regulators of pH as well as monovalent cation homeostasis (35). These carriers are expressed in cell- and subcellular-specific patterns, performing Na^+ exchange for H^+ down their respective concentration gradients in an electroneutral manner (e.g., $1Na^+:1H^+$) (4,32). NHEs display classical Michaelis-Menten kinetics with respect to the main extracellular cation Na^+ until exchangers are fully saturated (Fig. 2C) (34). By exhibiting a positive cooperative binding of intracellular H^+, NHEs can be triggered on and off rapidly in response to slight changes in intracellular acidity. Besides Na^+, ions such as Li^+, K^+, and ammonium (NH_4^+) are also transported by some NHEs/NHAs (34).

The NHEs have a relatively similar homodimeric structure as determined by biochemical (36,37) and cryo-EM methodology, studied best using the NHE1 isoform (38,39). The first two subfamilies, encoded by SLC9A1-9/NHE1-9 and SLC9B1-2/NHA1-2, possess a membrane topology with 12 relatively conserved transmembrane α-helices (plus a re-entrant loop structure that adds 2 additional membrane-embedded α-helices) at their amino-termini that confer ion translocation, along with less-conserved carboxy-termini involved in regulation, sorting and communication with other proteins (Fig. 2B) (34,40). By contrast, the third subfamily of NHEs, encoded by SLC9C1-2/NHE10-11 are thought to consist of 14 transmembrane α-helices in the amino-terminus along with a carboxy-terminus that contains 4 additional transmembrane helices that form a voltage-sensor domain and a distal cyclic-nucleotide-binding (CNB) domain facing the cytoplasm (41).

Within the SLC9 family, SLC9A1-9/NHE1-9 have been studied more extensively because of their involvement in many crucial cellular processes affecting adhesion, migration, proliferation, survival and apoptosis (42). Disruption of their normal function has been linked to many diseases, including diabetes, high blood pressure, congenital secretory diarrhoea, infertility, tumour growth and neurological conditions including brain ischemia/reperfusion damage and intellectual disability (42–46). Thus, there is an increasing effort to better understand the functioning of these transporters in order to develop therapeutic approaches to combat these conditions.

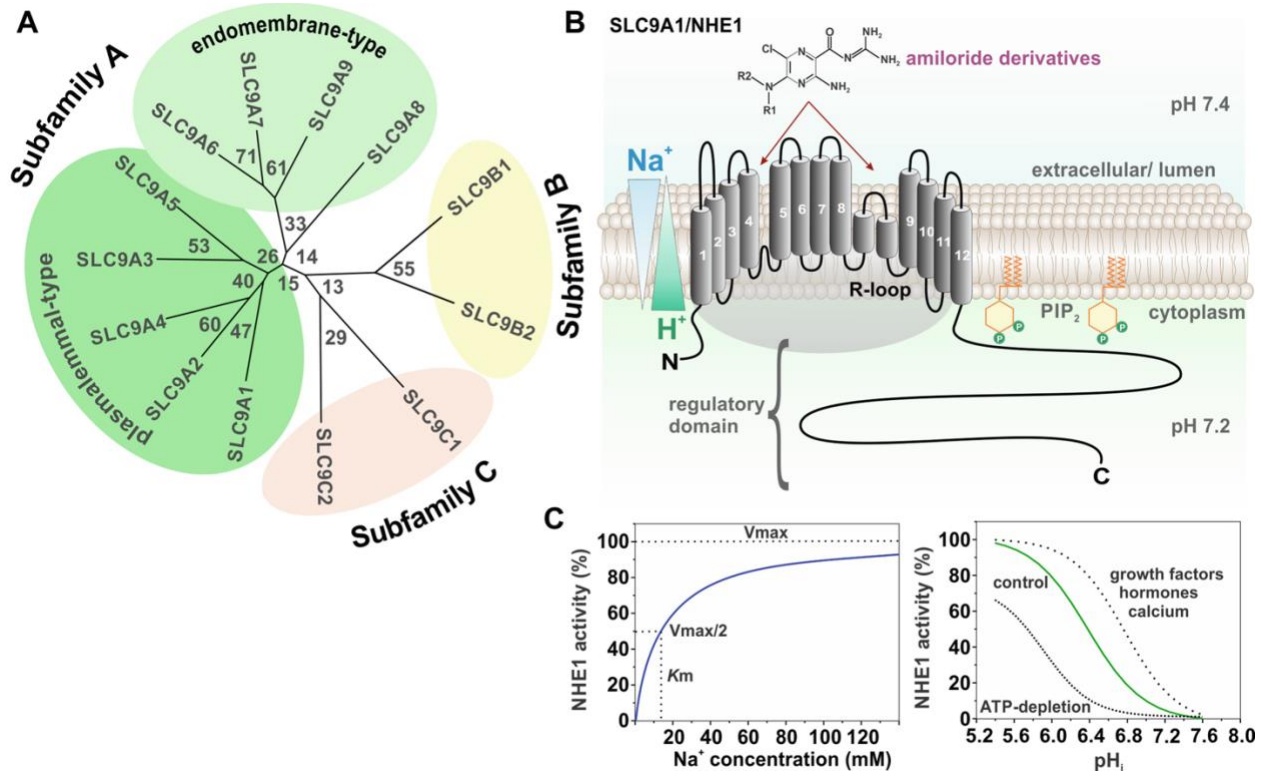

Figure 2 Basic characteristics of the SLC9/NHE gene family
(A) Genetic diversity and percent amino acids identity of SLC9/NHE isoforms. (B) Predicted transmembrane typology of NHE1, the prototype for most of the other NHE isoforms. Amiloride and amiloride-like analogues display inhibitory actions on sodium channels (C) Kinetic behavior of NHE1. Figure permission obtained from *Springer Nature, 2021* (31).

1.3 SLC9A Subfamily

The largest subfamily of NHEs can be segregated according to their subcellular localization. NHE1-5, encoded by *SLC9A1-5*, are typically active at the plasma membrane and depending on the isoform, appear in different cell types (32). As these transporters are not the focus of this thesis, they will not be further discussed. However, for more information, the reader is directed to previous reviews that have extensively documented their molecular, biochemical, and physiological properties (32,35). NHE6-9, encoded by *SLC9A6-9*, are classified as organellar or endomembrane NHEs as they are differentially localized to discrete intracellular compartments (Figure 3). This subset of NHEs is more relevant to my research project and hence are discussed in further detail below.

1.3.1 Endomembrane NHEs

NHE6: The focus of this research project is NHE6 which is expressed in all tissues but is particularly abundant throughout the central nervous system (47). This isoform controls pH homeostasis as well as membrane trafficking of early and recycling endosomes (34,44). Mutations in *SLC9A6* have been associated with Christianson Syndrome (CS), an X-linked neurodevelopmental disorder marked by developmental delay, epileptic seizures, ataxia, hyperkinetic behaviour, and degeneration of cortical, hippocampal, and particularly cerebellar neurons (48,49). The loss of NHE6 in most cases leads to excessive acidification of early and recycling endosomes and increased degradation of associated cargo, including neurotrophic (e.g., tropomyosin receptor kinase B (TrkB), also known as tyrosine receptor kinase B) and ionotropic (e.g., α-amino-3-hydroxy-5-methyl-4-isoxazolepropionic acid (AMPA)) receptors in hippocampal neurons of *Nhe6* knockout (KO) mice (50,51). These changes are thought to underlie some of the

neurological deficits. As a result, the strength and synaptic plasticity of these neurons are compromised, along with diminished dendritic arborization and mature dendritic spine density (51). Other neurological pathologies, including Alzheimer's disease, have also been connected to decreased NHE6 expression and activity (43,52,53). Amyloid beta (Aβ), a key contributor to amyloid plaque formation seen in the disease, was produced and secreted from endosomes more effectively when the endosomal pH was hyperacidic, which is associated with lower NHE6 activity (43).

NHE7: NHE7 is ubiquitously transcribed, with the highest expression occurring in the brain, skeletal muscle and various secretory tissues (54,55). Within cells, NHE7 localizes mainly within the *trans*-Golgi network (TGN) as well as post-Golgi vesicles and minimally at the cell surface (55). Here, the exchanger functions to regulate the organellar pH ranging from ~6.0 to 6.7. NHE7 associates with SCAMP2, a member of the secretory carrier associated membrane proteins (SCAMPs) (56). Ablation of SCAMP2's binding region for NHE7 causes an improper distribution of NHE7 to distinct recycling vesicle pools (56). These findings suggest that the NHE7-SCAMP2 interaction complex is necessary for proper shuttling of NHE7 between the TGN and recycling vesicles. A recent genetic study from our lab and collaborators also identified a recurrent *de novo* missense variant (L515F) within a highly conserved region of transmembrane helix 12 of NHE7 that is associated with a non-syndromic form of intellectual disability (57). This variant caused hyper-alkalinization of the TGN and impaired glycosylation of cargo that transits through the Golgi. This behaviour suggests a gain-of-function, though further studies are required to validate this possibility (57).

NHE8: NHE8 is widely expressed in mammals, with abundant levels observed within kidney and intestinal epithelial cells (58–60). Specifically in the proximal tubule of the kidney, NHE8 has been speculated to play a role in apical membrane reabsorption of salt (NaCl) and sodium bicarbonate ($NaHCO_3$) (40,58,61). Apart from epithelial apical membranes, NHE8 localizes to the TGN and MVBs in most cells (62). Depletion of NHE8 through siRNA knockdown technology revealed a significant increase in perinuclear clustering of endosomes and MVB (62). Recent data suggests NHE8 absence results in a syndrome that resembles ulcerative colitis with dysbiosis and decreased mucin synthesis, suggesting that NHE8 is crucial for intestinal mucosal defence (63).

NHE9: NHE9 is ubiquitously expressed, with the highest protein levels in the heart, skeletal muscle and brain (64,65). It is localized mainly to early and recycling endosomes, and sometimes partially overlaps with its other isoform, NHE6 (46). It has been proposed that defects in either NHE6 or NHE9 can be compensated by the other respective isoform, but evidence supporting this contention is lacking (46,66). Patients carrying mutations in *SLC9A9* have been linked to attention-deficit hyperactivity and autism spectrum disorders in humans, as moderate NHE9 levels are expressed in the brain (67–70).

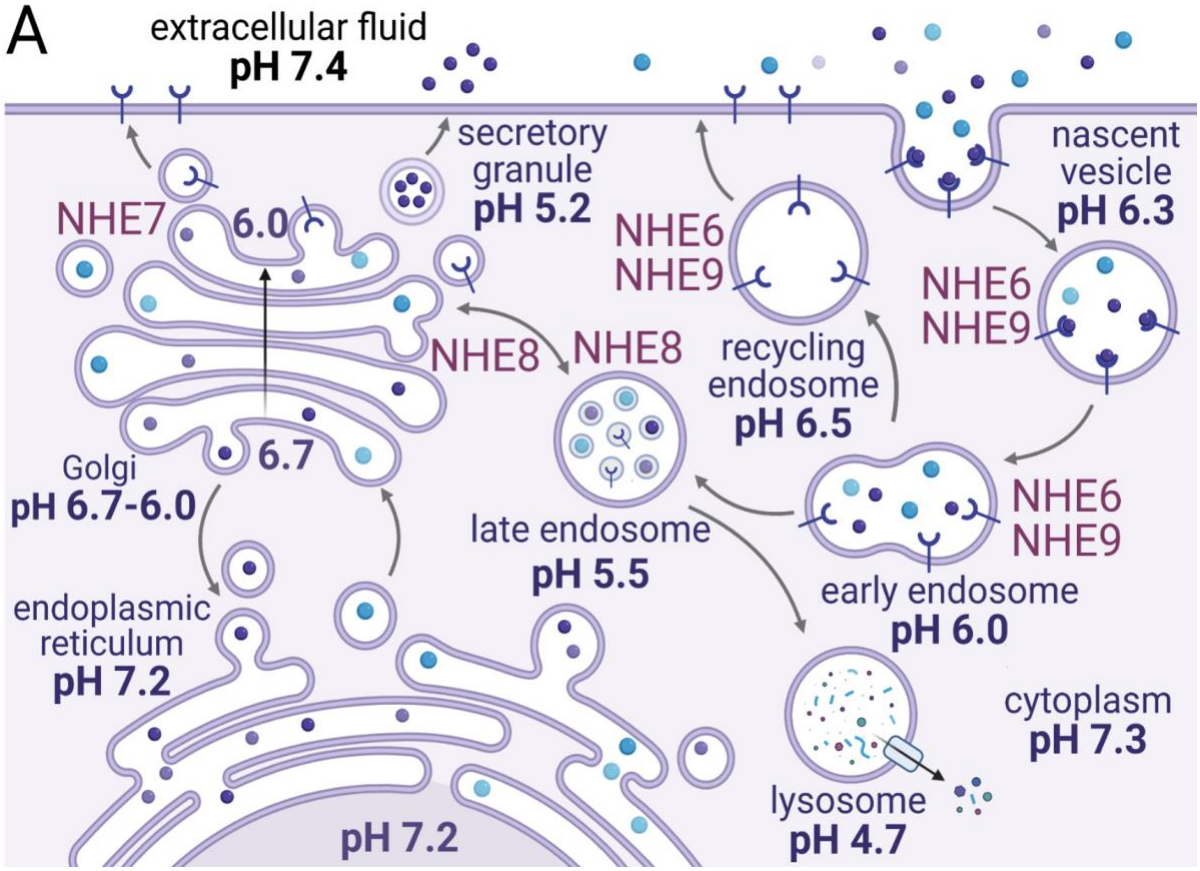

Figure 3 Subcellular localization of organellar NHE6-9, pH-regulating ion carriers
NHE6 and NHE9 localize to early and recycling endosomes, NHE7 localizes within the *trans*-Golgi network and post-Golgi vesicles. NHE8 localizes to late endosomes. Image created with BioRender.

1.4 NHE6 And Christianson Syndrome

Christianson syndrome (CS) was first described in 1999 (71), but the underlying genetic defect (i.e., *SLC9A6/NHE6*) was only discovered in 2008 by Gillifan *et. al* (72). Since then, over 110 distinct disease-causing mutations in *SLC9A6* have been documented (see databases ClinVar https://www.ncbi.nlm.nih.gov/clinvar/ and DECIPHER https://decipher.sanger.ac.uk/). A large-scale resequencing screen in patients with X-linked intellectual disabilities (XLID) indicated that *SLC9A6* is in the top 6 of a total of 141 mutated genes related to XLID (48,73,74). Its population frequency is estimated to be between 1:16,000 and 1:100,000 but may be higher due to misdiagnosis (48). Being an X-linked disorder, the disease affects primarily males, whereas female carriers are either asymptomatic or experience milder symptoms (75–77).

Studies of patients with CS have defined a core set of symptoms that occur in >85% of affected individuals. Besides intellectual disability, symptoms coinciding with those from Angelman syndrome are observed, such as mutism, postnatal microcephaly, epilepsy, cerebellar atrophy, truncal/gait ataxia and hyperactivity (48,49,78,79). Secondary symptoms can include convergent strabismus, hypotonia progressing to spasticity, cranial-facial anomalies, difficulty swallowing, a slender build and a high pain threshold (48,72). Laboratories studying the effects of CS typically involve investigating different regions of the brain.

The hippocampus is a complex brain structure that plays a major role in learning, memory consolidation, and spatial navigation (80). Our laboratory in collaboration with Dr. Anne McKinney's group was the first to show that NHE6 localizes to vesicles along axons and dendrites of hippocampal pyramidal neurons, with specific accumulation in most (~80%) postsynaptic dendritic spines and a majority (~60%) of presynaptic boutons (81). NHE6 is co-localized with typical markers of recycling endosomes, such as the transferrin receptor (81,82). Interestingly,

NHE6 also showed significant colocalization with the GluA1 subunit of the AMPA receptor at dendritic spines. Furthermore, NHE6-containing vesicles accumulated in postsynaptic dendritic spines upon glycine-mediated N-methyl-D-aspartate (NMDA) receptor-dependent long-term potentiation (LTP). LTP is a key cellular mechanism in learning and memory (83). The localization of NHE6 at glutamatergic synapses located in the dendritic spine heads suggests the exchanger plays a crucial role in activity-dependent stimulation of LTP, and its disruption can account for some of the deficiencies in neuronal development in patients harboring *SLC9A6* mutations (81).

Another important article implying NHE6 function is crucial for neuronal development was published in 2013 by Ouyang and colleagues (50). For the developing brain, strict control of axon and dendritic branching is critical for proper neuronal circuitry and function. This process is influenced by various signaling pathways, including endosomal signaling via the brain-derived neurotrophic factor (BDNF)/TrkB pathway which is critically involved in neuronal arborization and development (84,85). Ouyang and colleagues demonstrated that genetic ablation of *SLC9A6* in mice resulted in over-acidification of the endosomal compartment and attenuated TrkB signaling in cultured primary mouse hippocampal neurons (50). Loss of NHE6 in mice significantly reduced axonal branching and the number of mature dendritic spines of hippocampal neurons (50). Exogenous BDNF treatment of these mutant neurons significantly rescued axonal and dendritic branching, and thus may serve as a therapeutic strategy to treat CS patients.

A common symptom in patients with CS is hypoalgesia, or a lower sensitivity for pain (48). This is a great concern for parents of affected individuals as accidental injuries can possibly go unnoticed and unreported (due to patient mutism) and therefore delays treatment options. Mice lacking NHE6 also exhibit significant decreases in nocifensive responses to acute noxious thermal, mechanical, and chemical stimuli when compared to wild-type mice (86). NHE6 expression

analysis revealed significant levels in nociceptors of the dorsal root ganglia (DRG), one of the main areas associated with processing pain (86). Decreased nocifensive responses were attributed to NHE6's proposed interaction with transient receptor potential cation channel subfamily V member 1 (TRPV1), a channel present at the membrane of nociceptors, neurons associated with sensing pain.

Recently, scientists from the universities of Utah and Sydney recently identified the Shaker rat as a spontaneous model for studying CS. The rat, harboring a frameshift mutation in *SLC9A6,* leading to a truncated loss of function of NHE6, displayed symptoms of ataxia characterized by Purkinje cell loss (87). By performing intracerebroventricular injections containing an adeno-associated virus (AAV) targeting *SLC9A6* expression to Purkinje cells, a restorative phenotype was observed. Purkinje cell function returned to adequate levels, highlighting AAV-based gene therapy as a possible therapeutic strategy in the future (87).

Although most of the variants of *SLC9A6* observed in patients with CS lead to a non-functional NHE6 protein and thus a hyperacidic environment within endosomes, one variant investigated by our research lab, G218R, exhibited impaired endolysosomal trafficking and hypoacidification of recycling endosomes, revealing the diversity of dysfunctions originating from NHE6 (88).

To summarize, our lab and fellow collaborators have extensively studied NHE6 and its role in endosomal trafficking and CS. Excess acidification of endosomes, reduced trafficking of selected cargo, impaired oligosaccharide maturation and decreased stability/half-life of NHE6 are the most consistent findings with abnormal NHE6 function. However, other neurological pathologies, including Alzheimer's disease, have also been connected to decreased NHE6 expression and activity, speculating a much larger and more important role in neuronal function.

1.5 Research project, Hypothesis and Rationale

At present, the factors that govern the regulation and actions of NHE6 are poorly understood. ***We hypothesize that subcellular localized NHE6 and closely interacting proteins are a molecular link between the control of endosomal pH and trafficking signals that direct cargo needed for neurons to mature, function, and survive.*** Therefore, identifying the molecular network of NHE6's interacting proteins will potentially reveal novel NHE6-directed pathways crucial for neurons to exert their proper functions. We anticipate that such knowledge will help guide research and open new ideas into the impact of NHE6 on recycling endosomal pH homeostasis and trafficking.

We propose that NHE6 function is controlled and regulated by protein-protein interactions (PPI) occurring within its long-spanning C-terminus end, as the latter is known for communication with other proteins (34,40). In unpublished studies, our lab performed a yeast two-hybrid screen of a human brain cDNA library to identify putative NHE6 interacting proteins (*Ilie, A. and Orlowski, J., unpublished data*). However, a limitation of this approach is that it captures only stable protein-protein interactions, excluding many weak or transient associations that may be involved in a particular protein's interaction network (89). To solve this limitation and to gain further mechanistic insight into the factors that govern the trafficking and regulation of NHE6, we have adopted a technique for proximity-dependent labeling of proteins with biotin in eukaryotic cells (termed BioID for proximity-dependent biotin identification).

1.5.1 BioID

BioID is a cutting-edge technology used to unravel and scan for physiologically relevant protein-protein interactions (90). Introduced in 2012, BioID encompasses a range of techniques

used to identify and analyze various biological entities, including proteins, genes, and interactions within cellular systems (90,91). At its core, BioID relies on a process called proximity labeling with biotin. Researchers engineer a target protein of interest by fusing it with a promiscuous modified biotin ligase to the protein's N- or C-terminus (90). When the target protein comes into close vicinity with other proteins or molecules, the ligase enzymatically attaches a biotin molecule to them. Biotin serves as a molecular tag, allowing for subsequent isolation and identification of the labeled proteins through affinity purification by binding non-covalently to streptavidin, the latter naturally having a strong affinity for biotin. The isolated proteins are then identified by mass spectrometry.

By applying BioID to living cells or organisms, researchers can gain valuable insights into protein-protein interactions, protein localization within subcellular compartments, and dynamic changes in protein complexes under various conditions (90). This information helps to elucidate intricate cellular pathways, protein networks, and signaling cascades, contributing to a better understanding of fundamental biological processes and disease mechanisms. Furthermore, BioID can identify both stable and transient protein interactions and capture proteins in their native environments (90). Its versatility and ability to generate comprehensive interaction maps make BioID an invaluable tool for research, paving the way for discoveries relating to novel therapeutic interventions and targeted drug development (90).

Over the years, several types of BioID have emerged. Originally, the biotin ligase used was the BirA enzyme, derived from *E. coli* (91). BirA catalyzes the activation of biotin groups into 5'-AMP-biotin using ATP; the released 5'-AMP-biotin product can biotinylate almost any proximal protein (91). A modified version called TurboID emerged soon after researchers desired a shorter biotin incubation time for optimization, since the first method required an 18 h period. TurboID

optimized the speed and efficiency of labeling, demonstrating faster labeling kinetics, enabling shorter experimental timeframes (10-minute biotin incubation) while maintaining high specificity (92,93). Recent work has identified the use of peroxidases, such as horseradish peroxidase (HRP) and ascorbate peroxidase (APEX) as a new viable way to identify proximal proteins with BioID (94,95).

1.5.2 BioID using APEX2 with NHE6

Our lab designed a biotin ligase fusion construct for our protein of interest, human NHE6, with the latest version of the engineered ascorbate peroxidase, APEX2 (91). We used the long transcript splice-variant of human NHE6 as it is the most commonly occurring isoform *in vivo* (NHE6v1; NCBI RefSeq NM_001042537) (51,88,96). Upon expression in cells, the NHE6-APEX2 chimera will be induced to biotinylate interacting and proximate proteins using membrane-permeant biotin-phenol (BP) as substrate and hydrogen peroxide (H_2O_2) as a catalyst over a very brief period (1 minute) (97–99). The generated biotin-phenoxyl radical is a highly reactive and short-lived (<1 ms) species that binds to electron-rich amino acids such as tyrosine on neighboring proteins close to the APEX2 active site (within ~20 nm), thus generating a catalogue of biotinylated neighboring proteins (Figure 4) (97,100). These biotinylated proteins are subsequently purified using streptavidin-coated beads and identified via mass spectrometry (MS). This is the fastest method to date out of the various types of BioID and unlike other conventional methods used to screen for strong protein-protein interactions, such as co-immunoprecipitation, this method allows for the detection of weak and transient interactions within a relevant physiological milieu over a defined period of time, ideal for studying NHE6 (90).

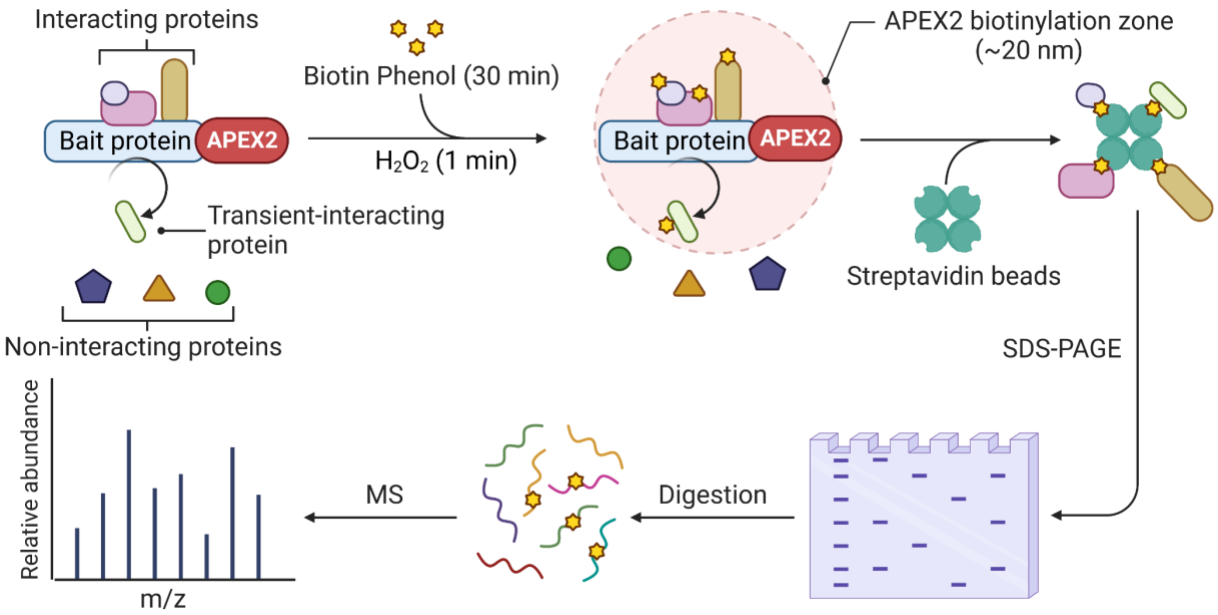

Figure 4 Step-by-step illustration of APEX2 experiment
APEX2 is attached to a protein of interest. Following a 30-minute incubation with biotin-phenol and sequential one-minute incubation with hydrogen peroxide (H_2O_2), APEX2 biotinylates nearby/interacting proteins in its ~20 nm labelling radius. Biotinylated proteins are isolated and purified with streptavidin beads. Samples are either run on a western blot for visualization or prepared for mass spectrometry identification. Identification is achieved through peptide mass fingerprinting. Image created with BioRender.

1.5.3 Research Objectives

My research project is comprised of several objectives. ***Aim 1:*** *To generate stable cell lines expressing NHE6-APEX2 constructs*. This will be accomplished by fusing APEX2 to the C-terminal end of the human NHE6v1 construct along with an intervening triple FLAG-tag (NHE6$_{3F}$-APEX2) and antibiotic resistance selection using geneticin (G-418) in a mammalian expression plasmid, pcDNA3. A single FLAG-tagged APEX2 construct ($_{1F}$APEX2) will be transfected in parallel and serve as a control. Human neuroblastoma SH-SY5Y cell lines will then be used as host cells for both chimeras. ***Aim 2****: To confirm the expression of the working constructs NHE6$_{3F}$-APEX2 and $_{1F}$APEX2 and verify that their subcellular localization is correct.* Western blots using a monoclonal FLAG antibody will be performed to confirm that the NHE6$_{3F}$-APEX2 and $_{1F}$APEX2 constructs have been stably integrated into the respective cell lines. The proper subcellular localization of our constructs will be confirmed by dual immunolabelling confocal fluorescence microscopy with appropriate marker proteins for recycling endosomes (i.e., transferrin receptor). ***Aim 3:*** *To identify which proteins are in the regional proximity of NHE6 through a small-scale proximity assay*. We will use H_2O_2 to catalyze the reaction of APEX2 in our constructs after the addition of BP, creating an oxidized biotin-phenoxyl radical that will biotinylate proximal endogenous proteins. We will confirm the identity of these tagged proteins by western blotting and mass spectrometry. ***Aim 4:*** *To follow up on one of the identified proteins and confirm the suspected interaction.* We will perform a co-immunoprecipitation assay to visualize if the suspected interaction forms a complex. In addition, a glutathione S-transferase (GST) pulldown assay using glutathione Sepharose beads will be used to determine the specific binding site of the protein to NHE6's C-terminus. By locating the specific binding region of a protein to NHE6's C-terminus, subsequent studies can be performed to investigate its importance

in greater detail. An example of a subsequent study would be to mutate or completely ablate the binding site, thus interrupting the interaction complex and revealing its potential role in receptor trafficking or the maintenance of organellar pH homeostasis.

EXPERIMENTAL PROCEDURES

2.1 Materials and Other Reagents

Alpha-minimum essential media (α-MEM), fetal bovine serum, penicillin/streptomycin, and trypsin-EDTA were purchased from Wisent (Saint-Bruno, QC, Canada). DMEM/F12 medium was purchased from Corning (#10-090-CV). The cOmplete^{TM} protease inhibitor cocktail tablets used in lysis buffers were purchased from Roche Diagnostics (#34045200). Co-immunoprecipitation experiments used Protein A Agarose beads from Invitrogen (#15918-014). Unless noted otherwise, all other chemicals and reagents were obtained from BioShop Canada, Sigma-Aldrich, or ThermoFisher Scientific and were of the highest grade available.

2.2 Antibodies

The following mouse monoclonal antibodies were used: anti-beta tubulin (T0198, Sigma-Aldrich), anti-hemagglutinin (HA) (901514, Biolegend), anti-FLAG (F3165, Sigma-Aldrich), anti-MYC (05-419, Millipore) and HRP-conjugated streptavidin (S911, Invitrogen). A specific rabbit polyclonal NHE6 antibody was generated by our lab against the NHE6 C-terminal tail, as previously described (81). For immunoblotting, horseradish peroxidase (HRP)-conjugated goat anti-mouse and anti-rabbit secondary antibodies were purchased from Jackson ImmunoResearch Laboratories. For fluorescence microscopy, Alexa Fluor® 488-conjugated goat (#A11001) and Alexa Fluor® 568 goat (#A11001) anti-mouse anti-rabbit secondary antibodies were purchased from Invitrogen.

2.3 Recombinant DNA constructs and mutagenesis

The long splice-variant transcript of human NHE6 (NHE6v1; NCBI RefSeq NM_001042537) was cloned from a human brain Matchmaker™ cDNA library (Clontech) using polymerase chain reaction (PCR) methodology and was engineered to contain the triple-FLAG ($_{3F}$) (3x DYKDDDDK) epitope at its extreme C-terminal end followed by APEX2 cDNA (encoding a 27 kDa protein). This construct was termed NHE6$_{3F}$APEX2 and inserted into the HindIII and XbaI sites of the mammalian expression vector pcDNA3 (Invitrogen). A control construct was also engineered, termed Flag-APEX2, containing a single FLAG epitope (DYKDDDDK), followed by APEX2 and inserted into the HindIII and XbaI sites of the mammalian expression vector pcDNA3 (Invitrogen). Another NHE6v1 was engineered to contain the influenza virus hemagglutinin (HA) (YPYDVPDYAS) epitope at its extreme C-terminal end (NHE6-HA) was inserted into the HindIII and XbaI sites of the mammalian expression vector pcDNA3 (Invitrogen).

2.4 Mammalian Cell Cultures and Transfections

Chinese hamster ovary (CHO) AP-1 cells were cultured in α-MEM with a pH of 7.4, containing 10% fetal bovine serum, penicillin (100 units/mL) and streptomycin (100 μg/mL). AP-1 cells stably expressing NHE6$_{3F}$APEX2 or $_{1F}$APEX2 were additionally supplemented with Geneticin (G418) (0.5 mg/mL) as a selection agent. Human neuroblastoma SH-SY5Y cells were grown in Dulbecco's Modified Eagle Medium (DMEM)/Ham's F12 medium supplemented with 10% fetal bovine serum and supplemented with Geneticin (G418) (0.5 mg/mL) as a selection agent. All cells were grown at 37℃ in a humidified chamber containing 5% CO_2.

Transient and stable transfections were carried out using 2.5 μL Lipofectamine2000™ (Invitrogen) per 1 μg of DNA or via Lonza's 4D-Nucleofector System™ according to the

manufacturer's recommendations. For lipofection, DNA and Lipofectamine were mixed in separate tubes of serum-free (or reduced serum) media. After 5 minutes, the Lipofectamine and DNA solutions were combined, and the resulting mixture was incubated at room temperature for 20 minutes. After rinsing the cells once, the media was replaced with serum-free media, and the transfection mixture was added to the cells. AP-1 cells were transfected in serum-free α-MEM, whereas SH-SY5Y transfections were carried out in Opti-MEM™ reduced serum medium (31985, Gibco). The transfection mix was replaced with full media (α-MEM for AP-1 cells or DMEM/F12 for SH-SY5Y cells) after 5 h, and cells were prepared for experiments 24 h post-transfection.

2.5 SDS-PAGE and Immunoblotting

For western blot analysis, cells were cultured in 2- or 10-cm dishes and transfected with a total of 2 or 8 μg of DNA, respectively. Cells were lysed 24 h post-transfection as follows: cells were rinsed twice in ice-cold phosphate-buffered saline (PBS) and scraped off dishes in lysis buffer (1% NP-40, 0.5% sodium deoxycholate, and cOmplete™ protease inhibitor cocktail dissolved in PBS). Cells in 2-cm dishes were lysed in 100-200 μL lysis buffer, whereas cells in 10-cm dishes were lysed in 450-650 μL lysis buffer, depending on the confluency of the dish. Cell lysates were then rocked for 30 minutes at 4℃ and centrifuged at 16,100 x *g* for 20 minutes to remove nuclei and cell debris. The protein concentrations of the supernatants were measured using Bio-Rad DC™ Protein Assay reagents or Pierce™ Protein Assay reagents.

Equal amounts of protein were prepared in sodium dodecyl sulphate (SDS) sample buffer (50 mM Tris-HCl, pH 6.8, 1% SDS, 50 mM dithiothreitol (DTT), 10% glycerol, 1% bromophenol blue), subjected to gel electrophoresis on 9-12% SDS-polyacrylamide (PAGE) gels, and transferred to polyvinylidene fluoride (PVDF) membranes (10600023, GE Healthcare).

Membranes were blocked with 5% non-fat skim milk for 1 h at room temperature or 3% bovine serum albumin in tris-buffered saline (TBS) and 0.1% Tween 20 overnight at 4℃. The membranes were then incubated with specific primary antibodies in a PBS solution containing 5% non-fat skim milk and 0.1% Tween 20, followed by washes (4 x 10 minutes) in PBS containing 0.1% Tween 20 (PBS-Tween) or in 3% bovine serum albumin in TBS and 0.1% Tween 20. The following primary antibodies were incubated for 1 h at room temperature: mouse monoclonal anti-HA 1:4000, anti-β-tubulin 1:20,000, anti-FLAG 1:4,000, anti-MYC 1:4,000, anti-streptavidin-HRP 1:10-20,000. The following primary antibodies were incubated overnight at 4℃: mouse monoclonal anti-MYC 1:1500 and rabbit polyclonal anti-NHE6 1:5000. Subsequently, all membranes were incubated with HRP-conjugated secondary antibodies for 1 h at room temperature (typically 1:4000 HRP-conjugated goat anti-mouse or 1:10,000 HRP-conjugated goat anti-rabbit), followed by extensive washes (2 x 10 minutes in PBS-Tween and 3 x 10 minutes in PBS). Finally, immunoreactive bands were detected using Western Lightning™ Plus-ECL blotting detection reagents (Perkin Elmer) and autoradiography films.

2.6 Immunofluorescence Confocal Microscopy

To visualize intracellular localization of the working NHE6$_{3F}$APEX2 construct into transferrin-containing recycling endosomes, SH-SY5Y cells stably expressing NHE6$_{3F}$APEX2 were plated on 18 mm fibronectin-coated glass coverslips (64-0714, Warner Instruments). Once grown to ~80% confluency, cells were then subjected to exogenous transferrin using Alexa Fluor® 594-conjugated transferrin (Tf-A^{594}) for 2 h in order to examine the internalization of transferrin within NHE6-containing vesicles. Then, cells were rinsed twice in PBS and fixed in 4% paraformaldehyde (PFA) for 20 minutes at room temperature.

Samples were then rinsed 4 times in PBS to remove excess PFA and permeabilized in 0.1% saponin for 20 minutes. After rinsing once, cells were blocked for 1 h in a blocking solution (10% goat serum, 0.01% saponin, and 0.1 M glycine in PBS). Next, cells were incubated with primary antibody overnight at 4℃ (rabbit polyclonal anti-NHE6 1:300, diluted in blocking solution), followed by several washes (4 x 10 minutes in blocking solution). Secondary antibodies used were Alexa Fluor® 488-conjugated goat anti-rabbit 1:1000 and Alexa Fluor® 568-conjugated goat anti-rabbit 1:1500, diluted in blocking solution. Samples were incubated with the latter for 1 h at room temperature and washed several times (4 x 10 minutes in PBS). For samples dyed with 4′,6-diamidino-2-phenylindole (DAPI), a 1:8000 dilution in PBS was incubated with samples for 15 minutes at room temperature, followed by washes (4 x 5 minutes) in PBS. Coverslips were then rinsed once in (distilled water) dH_2O and mounted on glass microscopy slides (48311- 601, VWR) using Aqua Poly/Mount (18606, Polysciences Inc.) mounting media.

All cells were imaged with laser scanning confocal microscopy using a Zeiss LSM 710 microscope equipped with a photomultiplier tube detector. Images were acquired using a 63 x /1.4 N.A. oil immersion objective lens with the following lasers: 488 nm Argon-Ion, 568 nm Diode-Pumped Solid-State (DPSS), and 405 nm blue diode. All images were acquired as Z-stacks and are displayed as maximum-intensity projections. The same acquisition parameters were used for all cells of a given trial, and for transfected cells, only low-to-medium expressing cells were imaged.

2.7 APEX2 assay for mapping NHE6 interacting proteome

For western blot verification, cells were cultured in triplicate in 35-mm dishes and grown to confluence. Once confluent, cells were re-fed with/without media containing 0.5 mM biotin-phenol (BP) in the following fashion: Wells 1 and 2: DMEM/F-12 with 0.5 mM BP, well 3:

DMEM/F-12. Following the 30-minute incubation, cells were washed 3x in PBS pH 7.2, and subjected to a 1-minute incubation of hydrogen peroxide or PBS in the following fashion: Well 1 and 3: 1 mM H_2O_2, well 2: PBS. Reactions were halted using a 2-step quenching buffer and subsequently lysed using a specific RIPA lysis buffer (0.5 M Tris pH 8.0, 1M NaCl, 0.5 M EDTA pH 8.0, 0.5% sodium deoxycholate, 0.1% SDS, 0.1% Triton X-100, 5 mM Trolox, 10 mM sodium ascorbate and 10 mM sodium azide). Quenching solution: PBS-CM pH 7.4, 5 mM Trolox, 10 mM sodium ascorbate, 10 mM sodium azide. Aliquots of lysates were diluted 1/10 with 9 parts lysis buffer and total protein was measured using the Pierce™ protein assay, measuring absorbances at 660 nm. Samples for western blot were mixed with 1× protein loading buffer, boiled for 10 minutes, rocked at room temperature for 30 minutes and run on 9% SDS-PAGE gel. Detection of biotinylated proteins and proper construct expression (as a control) was performed by immunoblotting following a ponceau S stain to inspect the quality of transfer (then removed with deionized water several times).

2.8 APEX2 assay for detection of NHE6 interacting proteome through mass spectrometry

Cells were cultured in 15-cm dishes. For each construct, 2 dishes were treated with biotin-phenol (BP) 0.5 mM + H_2O_2 1 mM and 2 dishes with BP 1 mM + H_2O_2 0.5 mM. Reactions were quenched and cells were lysed using 200-250 µl of lysis buffer containing 96% radioimmunoprecipitation (RIPA) buffer (50 mM Tris pH 8.0, 1 M NaCl, 5 mM EDTA pH 8.0, 0.5% sodium deoxycholate, 0.1% SDS and MilliQ water), protease inhibitor cocktail, 5 mM Trolox, 10 nM sodium ascorbate, 10 mM sodium azide. Lysis was performed on ice by gently pipetting, then lysates were rocked for 30 minutes at 4 degrees. Lysates were then spun down at 16,000 x *g* for 20 minutes at 4℃. Aliquots of cell lysates were aliquoted 1/10 and total protein

concentration was measured using the Pierce™ protein assay. Two milligrams of total cell lysates (TCL) were mixed with 350 µL NeutrAvidin™ agarose beads for 1.5 h at 4℃ on a rotator, and a lysis buffer containing the same volume was added. After the incubation, aliquots were spun at 500 x *g* for 2 minutes and supernatants were transferred to new tubes. These new aliquots were washed with 1 mL of RIPA buffer, 1 mL 1M KCl, 1 mL Na_2CO_3, 1 mL 2 M Urea in 10 mM Tris-HCl pH 8.0 and 1 mL RIPA buffer. Two-minute incubations while rocking were between each wash with 2-minute spins at 500 x *g*. Biotinylated proteins present on the beads were eluted by boiling each sample in 52 µl of elution buffer for 10 minutes following a brief vortex before and after boiling. Samples were cooled on ice, and spun down for 2 minutes at 500 x *g* and 50 µl of eluate was collected from each sample. Samples were then flash frozen in liquid nitrogen and stored at -80℃ until shipment to the Proteomics Facility at the McGill University Health Center – Glen Site.

2.9 Co-Immunoprecipitation

Cells were cultured in 10-cm dishes and transfected with a total of 5 µg of DNA. Twenty-four hours post-transfection, cells were rinsed twice in ice-cold PBS and scraped off dishes in 450-650 µL lysis buffer (1% NP-40, 0.5% sodium deoxycholate, and cOmplete™ protease inhibitor cocktail dissolved in PBS), depending on the confluency of the dish. Cell lysates were then rocked for 30 minutes at 4℃ and centrifuged at 16,100 x *g* to remove nuclei and cell debris. Supernatants were precleared on Protein A Agarose beads for 3 h. The beads were removed by centrifugation (5 min at 2,300 x *g*), and the supernatants were rocked at 4℃ overnight with ~2.5 µg of the rabbit anti-HA antibody. The supernatants were then rocked for 3 h at 4℃ with a 50% slurry of Protein A beads in lysis buffer. The beads were washed 6 times in 750-1000 µL lysis buffer, rocking for 2

minutes and centrifuging at 2,500 x *g* for 3 minutes in between washes. The immunoprecipitated complexes were eluted in 50 µL of SDS sample buffer (50 mM Tris-HCl, pH 6.8, 1% SDS, 50 mM DTT, 10% glycerol, 1% bromophenol blue) by rocking for 30 minutes at room temperature and centrifuging for 5 minutes at 17,000 x *g*. Finally, immunoprecipitated proteins were subject to SDS-PAGE on 10% gels, transferred to PVDF membranes and immunoblotting. Total cell lysates (TCL) were also resolved by SDS-PAGE and immunoblotted for $_{MYC}$RAC1, NHE6$_{HA}$, and β-tubulin (as a negative control).

2.10 Manders' Colocalization Analysis

ImageJ software was used to process images and quantify the colocalization of NHE6 and Tf-A^{594} containing vesicles in immunofluorescence confocal microscopy images. This was also performed to quantify the colocalization of RAC1 and NHE6. Images were cropped using the freehand selection tool so that only one cell was left in the field of view. The ImageJ JACoP plugin was used to apply thresholds to the NHE6 and Tf-A^{594} signals and measure Manders' colocalization coefficients (MCC). MCC were calculated as the percentage of pixels positive for signal A (e.g., NHE6) that are also positive for signal B (e.g., Tf-A^{594}).

2.11 Glutathione-S-Transferase Pull-Down Assay

Generation of glutathione-S-transferase (GST) fusion proteins: The coding sequences of various segments of the NHE6 C-terminal tail were previously cloned into the isopropyl-b-D-thiogalactoside (IPTG)-inducible expression vector pGEX-2T. BL-21 competent *Escherichia coli* was transformed with these plasmids; pGEX-2T without a DNA insert (*i.e.*, encoding only the GST protein) was also transformed as a negative control. Transformed BL-21 colonies were

inoculated in 3 mL of 2× yeast exact tryptone (YT) bacterial media supplemented with 100 μg/mL ampicillin and grown overnight at 37℃ with shaking. Then, 2 mL of the overnight bacterial cultures were inoculated in 50 mL 2× YT media with 100 μg/mL ampicillin and grown at 37℃ with shaking until the cultures reached an optical density of 0.8-0.9 at 600 nm (*i.e.*, OD_{600} = 0.8-0.9). The cultures were transferred to a 30℃ shaker for 10 minutes, and plasmid expression was induced with 1M IPTG for 3 h at 30℃ with shaking. The bacteria were then pelleted by a 20-minute centrifugation at 3,150 x *g* at 4℃. The supernatant was discarded, and pellets were resuspended in GST lysis buffer (0.5% NP-40, 1 mM EDTA, and cOmplete™ protease inhibitor cocktail dissolved in PBS). The bacteria were sonicated 2-4 times for 30 seconds on ice, with at least 1 minute between each sonication, and centrifuged for 30 minutes at 16,100 x *g* to remove bacterial debris. The supernatants were stored at -70℃ until further use.

Purification of GST fusion proteins to check expression levels: GST fusion proteins were purified from 100 μL bacterial lysates by rocking with a 50% slurry of glutathione Sepharose™ 4B beads (17-0756, GE Healthcare) in GST lysis buffer for 3 h or overnight at 4℃. To remove unbound proteins, the beads were washed 6 times in 1 mL GST lysis buffer, rocking for 2 minutes and centrifuging for 1 minute at 500 x *g* in between washes. The bound GST fusion proteins were eluted from the beads in 40 μL SDS sample buffer (50 mM Tris-HCl, pH 6.8, 1% SDS, 50 mM DTT, 10% glycerol, 1% bromophenol blue) by incubating at 90℃ for 5 minutes and centrifuging at 17,000 x *g* for 5 minutes. Finally, the eluted proteins were run on a 10% SDS-PAGE gel, visualized by coomassie blue staining for 40 minutes, and de-stained overnight in a 25% methanol, 10% acetic acid solution. The volumes of bacterial lysates needed for equal amounts of GST fusion proteins were qualitatively estimated from the stained gel.

GST pull-down assay: GST pull-down assays were performed with endogenous NHE6 from AP-1 $NHE6_{HA}$-stably expressing cells and GST fusion proteins containing various segments of the NHE6 C-terminal tail. AP-1 cells were grown on 10-cm dishes until confluent, rinsed twice in ice-cold PBS, and lysed in 450-650 µL RIPA lysis buffer (1% NP-40, 0.5% sodium deoxycholate, and cOmplete™ protease inhibitor cocktail dissolved in PBS). To purify the GST fusion proteins, appropriate volumes of BL-21 bacterial lysates were rocked for 3 h with Glutathione Sepharose™ beads at 4℃. The beads were washed three times in 1 mL GST lysis buffer, with 2 minutes of rocking and 1-minute centrifugation at 5,000 x *g* in between washes. 1000-1500 µg of AP-1 cell lysates were then rocked with the beads overnight at 4℃. The beads were washed 6 times with 1 mL RIPA buffer to remove extraneous proteins, and the remaining proteins were eluted from the beads in 50 µL SDS sample buffer by rocking for 30 minutes at room temperature and centrifuging at 17,000 x *g* for 3 minutes. Finally, the samples were subject to SDS-PAGE and immunoblotted for MYC-tagged fusion proteins, and the membrane was stained with Ponceau to verify the expression of the GST fusion proteins.

2.12 Cell Surface Biotinylation Experiment

AP-1 cells expressing $NHE6_{HA}$ or non-transfected AP-1 cells were cultured in 10-cm dishes to subconfluence, placed on ice, and washed three times with ice-cold PBS pH 8.0 containing 1 mM $MgCl_2$ and 0.1 mM $CaCl_2$. Next, cells were incubated at 4°C for 30 min with the membrane-impermeable reagent *N*-hydroxysulfosuccinimidyl–SS-biotin (0.5 mg/ml) (Thermo Fisher Scientific, Rockford, IL). Cells were washed and incubated twice in quenching buffer (50 mM glycine in PBS-CM) for 7 min each on ice to remove unreacted biotin. After two more washes in PBS-CM, the cells were lysed for 30 min on ice and then centrifuged at 16,000 *g* for 20 min at 4

°C to remove insoluble cellular debris. A fraction of the resulting supernatant was removed, and this represents the total fraction. The remaining supernatant was incubated with 100 µl of 50% NeutrAvidin–agarose resin slurry (Thermo Fisher Scientific, Whitby, Ontario, Canada) in lysis buffer overnight at 4 °C to extract biotinylated membrane proteins. The proteins were then resolved by SDS-PAGE and analyzed by western blotting.

2.13 Statistical Analysis

Data are presented as the mean ± the standard error of the mean (S.E.M.) unless noted otherwise. Statistical analysis was performed using a two-tailed Student's *t*-test. A minimum p-value of < 0.05 was considered statistically significant.

RESULTS

3.1 NHE6$_{3F}$APEX2 is properly expressed and colocalizes with typical markers of RE in human SH-SY5Y neuroblastoma cells.

The non-neuronal Chinese hamster ovary (CHO)-derived AP-1 cells are the typical cells of choice that we use in our laboratory. This cell line expresses low to negligible levels of endogenous NHE6 and possesses many of the constitutive and regulated protein sorting mechanisms found in polarized cells, such as epithelia and neurons (101–103). Our second cell line is the human neuroblastoma SH-SY5Y cell line, which we and others have previously shown expresses high levels of NHE6 relative to other NHEs (81,104,105).

Investigating the factors that govern NHE6 and its regulation can be suitably tested in both the AP-1 and SH-SY5Y cell lines, making them tractable model systems. These cell lines have the capacity to generate stably transfected cells, and the SH-SY5Y cells can be differentiated into a mature neuron-like phenotype for further biochemical analyses, on top of relative ease and efficient cost to culture compared to the use of primary neurons (106).

Stable expression of NHE6$_{3F}$APEX2 or the control construct $_{1F}$APEX2 in SH-SY5Y cells was obtained using either a liposomal-mediated (Lipofectamine) or an electroporation-based (Nucleofection) transfection method and antibiotic (G418) selection. Stably-expressing pools of cells were kept for further examination. Cells were grown to confluency and lysed in RIPA (radioimmunoprecipitation assay) buffer (composition listed in Methods).

For our initial screen, differentiated SH-SY5Y cell pools stably expressing comparable levels of $_{1F}$APEX2 and NHE6$_{3F}$APEX2 were selected to minimize expression level- and clonal isolate-based differences (Figure 5A). For NHE6$_{3F}$APEX2, three distinct protein bands were detected, consistent with previous literature (44,96). Specifically, bands were observed at ~240 kDa

representing the dimeric form of the exchanger that does not fully dissociate under SDS-PAGE conditions; at ~130 kDa representing the fully-glycosylated (fg) monomeric form; and at ~100 kDa; representing the core-glycosylated (cg) monomeric form of NHE6$_{3F}$APEX2 (Figure 5A). The control construct $_{1F}$APEX2 was also observed at the expected size of ~27 kDa (Figure 5A).

To distinguish native NHE6 from transfected NHE6$_{3F}$APEX2, cells were immunoblotted with a rabbit polyclonal anti-NHE6 antibody generated by our lab (81). The three different forms of native NHE6 can be properly distinguished from transfected NHE6$_{3F}$APEX2 due to their smaller sizes (Figure 5B). Western blotting showed that NHE6$_{3F}$APEX2 expression was ~2–3 fold higher than native NHE6 (Figure 5B), suggesting that most NHE6 expressed will form NHE6$_{3F}$APEX2 homodimers.

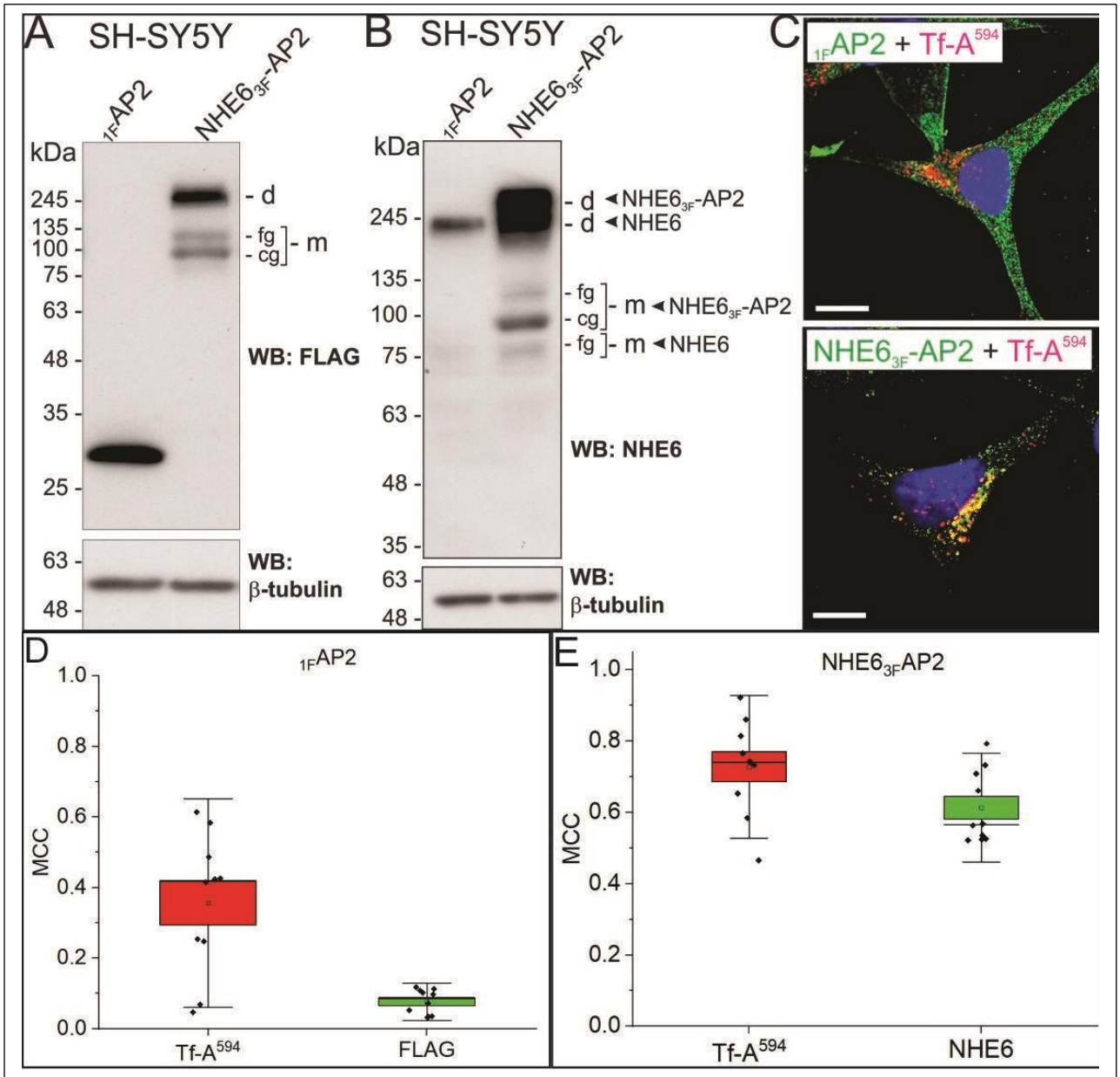

Figure 5 Expression and subcellular distribution of transfected constructs
(A-B) Stable expression of $_{1F}$APEX2 (abbreviated $_{1F}$AP2) and NHE6$_{3F}$APEX2 (abbreviated as NHE6$_{3F}$-AP2) in human SH-SY5Y neuroblastoma cells as well as endogenous NHE6 expression via detection of FLAG mouse monoclonal and NHE6 rabbit polyclonal antibodies, respectively, and β-tubulin for confirmation of equal protein loading. (C) Subcellular localization of $_{1F}$AP2 and NHE6$_{3F}$-AP2 constructs in transfected SH-SY5Y cells with Alexa Fluor® 594-conjugated transferrin (Tf-A^{594}) along with DAPI for nuclear staining (10 µm scale). (D-E) Quantitation of the degree of $_{1F}$AP2and NHE6$_{3F}$-AP2 overlapping with Tf-AF^{594} was determined by calculating the thresholded Manders' colocalization coefficients (MCC) (M1 and M2) using ImageJ software and the JACoP plugin. Data are plotted as a box chart, with the central white square indicating the mean, the box representing the S.E.M. and the error bars showing the S.D. (n = 10 cells). *t*-test *p*-value: $p = 1.1 \times 10^{-8}$.

The stable SH-SY5Y cell lines were next examined by immunofluorescence confocal microscopy to verify that the NHE6$_{3F}$APEX2 and $_{1F}$APEX2 constructs were properly sorted to recycling endosomes and cytoplasm, respectively. Representative images showed that $_{1F}$APEX2 (Fig. 5C, upper panel, in green) was distributed diffusely in the cytoplasm, as expected. Conversely, NHE6$_{3F}$APEX2 (Fig. 5C, lower panel, in green) accumulated mainly in perinuclear transferrin-Alexa Fluor® 594 (Tf-A^{594})-labelled recycling endosomes (in red, yielding a merged yellow signal), consistent with its native intracellular distribution. To quantify the degree of colocalization between NHE6$_{3F}$APEX2 and Tf-A^{594} in SH-SY5Y cells, Manders' colocalization coefficients (MCC) were calculated for both markers. MCC values range between 0 and 1, where 0 indicates no colocalization and 1 infers perfect colocalization. The mean MCC for NHE6 was approximately 0.73 ± 0.13, meaning 73% of NHE6-positive pixels were also positive for transferrin (Fig. 5E). Likewise, the MCC for transferrin was 0.61 ± 0.10, meaning 61% of Transferrin-positive pixels were positive for NHE6. These values indicate that the two proteins show moderate co-occurrence in recycling endosomes of SH-SY5Y cells, consistent with previous reports (44,96). The $_{1F}$APEX2 construct did not exhibit substantial co-localization with Tf-positive vesicles (Tf-A^{594} with FLAG: 0.07, 7%), as expected (Fig. 5C: top image, 5D) (97,100).

3.2 APEX2 assay reveals NHE6 proximate proteome

Western blot validation of APEX2-mediated biotinylation of proteins in SH-SY5Y cells stably expressing NHE6$_{3F}$-APEX2 or $_{1F}$APEX2 was conducted prior to mass spectrometry (MS) analysis (Fig. 6). MS analysis of the extracted biotinylated proteins was performed at the Proteomics Platform of the Research Institute of the McGill University Health Centre (RI-MUHC; https://rimuhc.ca/clinical-proteomics) using a Thermo Scientific Orbitrap Fusion^{TM} Mass

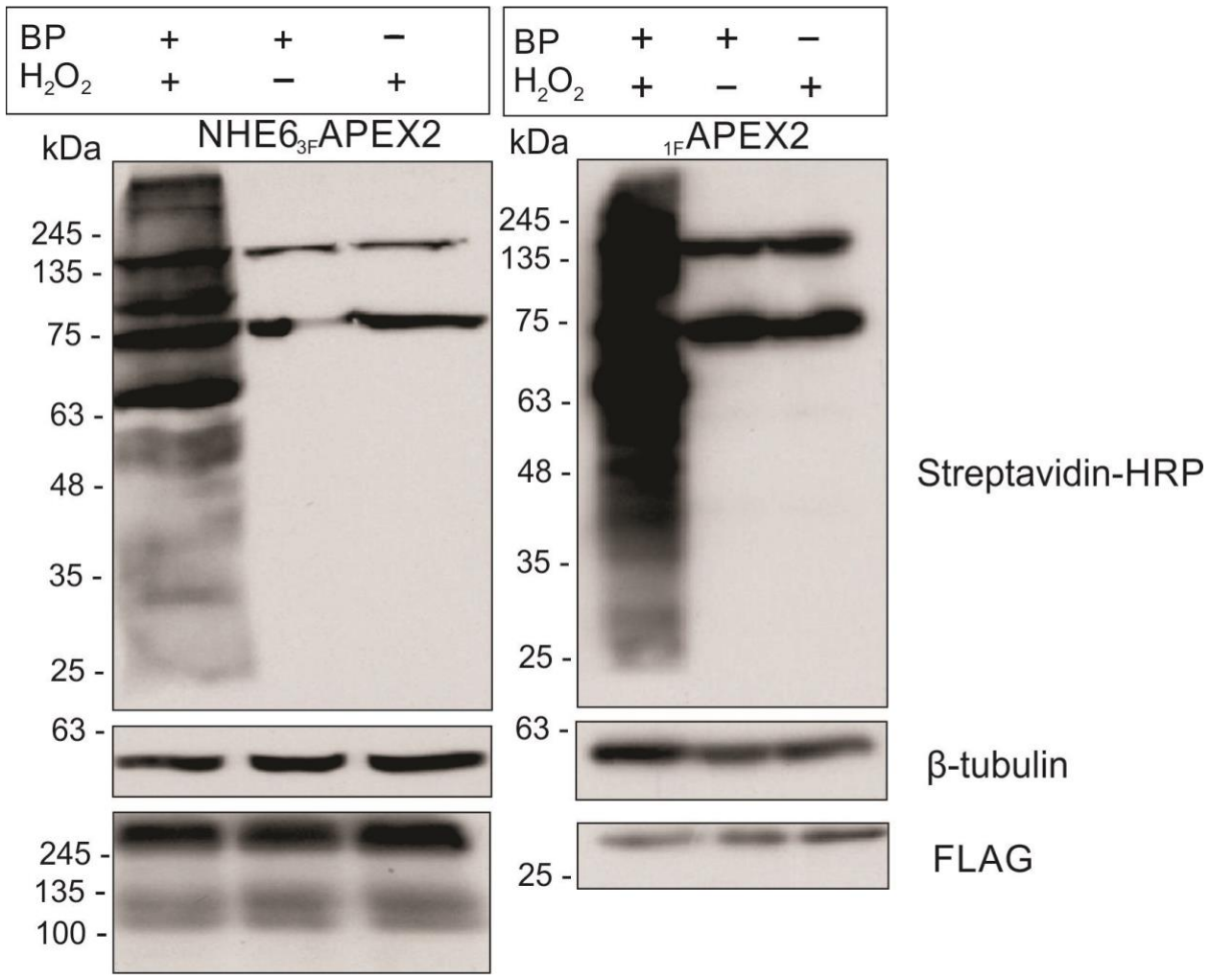

Figure 6 Western blot validation of APEX2-mediated biotinylation of proteins in SH-SY5Y cells

Broad range of defined bands corresponding to NHE6$_{3F}$-APEX2 and $_{1F}$APEX2 proteome in lanes subject with both biotin-phenol (BP) and hydrogen peroxide (H_2O_2). Negative controls in which either reactant was omitted (lanes 2 and 3) are shown. Presence of endogenous biotinylated proteins are observed in these lanes. Loading confirmation confirmed using monoclonal antibody for cytosolic β-tubulin and construct expression confirmed using the FLAG monoclonal antibody. This experiment was repeated in three separate trials.

Spectrometer. The identified peptides and corresponding proteins were loaded onto Scaffold Q+/Quant v5.0 (Proteome Software Inc.) for statistical treatment and data visualization. Our analyses identified 147 and 57 biotinylated proteins in the NHE6$_{3F}$APEX2 and $_{1F}$APEX2 stable transfectants, respectively (protein threshold 99%; min. #peptides 2; peptide threshold 95%), of which 51 proteins were common to both constructs (Fig. 7A). NHE6$_{3F}$APEX2 uniquely labelled 96 proteins. After excluding common background contaminants often detected in proteomic analyses (e.g., heat shock proteins, keratins, elongation factors, histones, ribosomal proteins, and four endogenously biotinylated carboxylase proteins (Acetyl-CoA Carboxylase (ACACA) (220 kDa), Pyruvate Carboxylase (PC) (130 kDa), β-methylcrotonyl-CoA carboxylase (MCCC1) (75 kDa) and Propionyl-CoA-carboxylase (PCCA) (72 kDa)), the list of putative candidates of the NHE6 proximate proteome was restricted to 66 proteins, including NHE6 (Table 1) (107–109). Proteins were subjected to Gene Ontology (GO) enrichment analysis using the ShinyGO graphical web application which includes interface access to the Kyoto Encyclopedia of Genes and Genomes (KEGG) and STRING analysis for the retrieval of protein-protein interaction (PPI) networks, clustering analysis and biological pathways (110–113). Specifically, NHE6$_{3F}$APEX2 biotinylated proteins that partitioned into several closely aligned GO biological processes, including actin cytoskeleton organization, neuron projection morphogenesis, synapse organization, and organelle localization, amongst others (Fig. 7B-C). Calculation of the PPI-enrichment p-value was <1.0e-16, indicating that the network and number of protein nodes (66) are not random and the observed # of 'edges' (347, expected 57; *edges (colored lines) represent documented evidence for predicted and functional associations*) are highly significant.

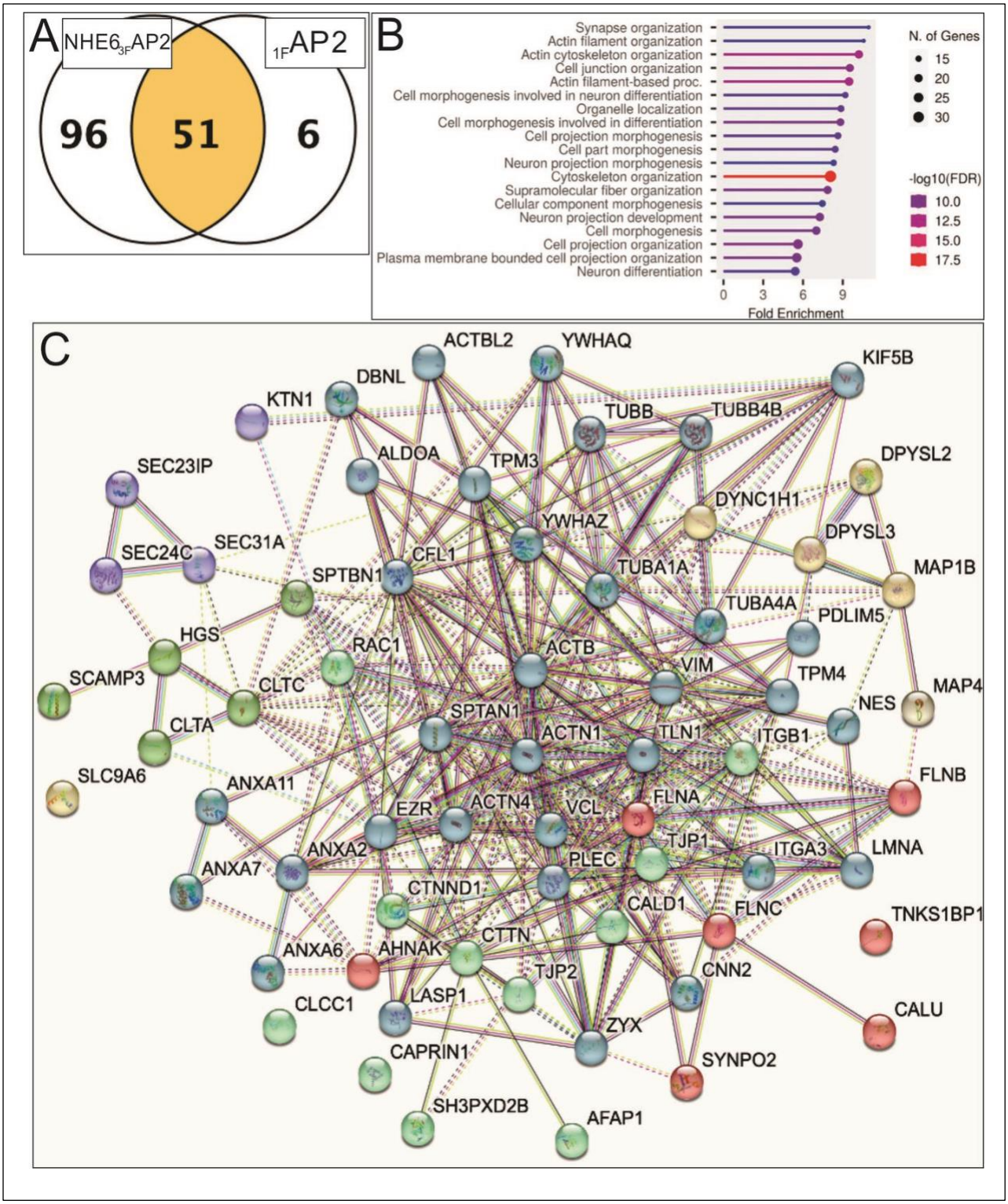
A
NHE6$_{3F}$AP2
$_{1F}$AP2
96
51
6
B
Synapse organization
Actin filament organization
Actin cytoskeleton organization
Cell junction organization
Actin filament-based proc.
Cell morphogenesis involved in neuron differentiation
Organelle localization
Cell morphogenesis involved in differentiation
Cell projection morphogenesis
Cell part morphogenesis
Neuron projection morphogenesis
Cytoskeleton organization
Supramolecular fiber organization
Cellular component morphogenesis
Neuron projection development
Cell morphogenesis
Cell projection organization
Plasma membrane bounded cell projection organization
Neuron differentiation
0
3
6
9
Fold Enrichment
N. of Genes
15
20
25
30
-log10(FDR)
10.0
12.5
15.0
17.5
C
ACTBL2
YWHAQ
KIF5B
DBNL
KTN1
TUBB
TUBB4B
ALDOA
TPM3
DPYSL2
SEC23IP
DYNC1H1
YWHAZ
DPYSL3
SEC24C
SEC31A
CFL1
TUBA1A
MAP1B
SPTBN1
TUBA4A
PDLIM5
HGS
RAC1
ACTB
VIM
TPM4
MAP4
SCAMP3
CLTC
NES
SPTAN1
CLTA
ACTN1
TLN1
ITGB1
SLC9A6
FLNB
ANXA11
EZR
ACTN4
VCL
FLNA
TJP1
ITGA3
LMNA
ANXA2
ANXA7
PLEC
CTNND1
CALD1
FLNC
TNKS1BP1
CTTN
ANXA6
AHNAK
TJP2
CNN2
CLCC1
LASP1
CALU
ZYX
CAPRIN1
SYNPO2
SH3PXD2B
AFAP1

Figure 7 Mass Spectrometry Analysis
(A) Venn diagram representing number of biotinylated proteins for each working construct. (B) Gene ontology and fold enrichment analysis of biotinylated proteins using the ShinyGO web application using the finalized list of 66 proteins that constitute the NHE6 proteome. (C) String-DB clustering map of NHE6 interacting proteins. Line sequence legend: Blue: known interactions from curated databases; Magenta: known interactions from experimental determination; Green: gene neighborhood of predicted interactions; Red: gene fusions of predicted interactions; Blue: gene co-occurrence of prediction interactions; undashed lines: cluster respective interactions; dashed lines: inter-cluster interactions. Protein color legend: Blue: Postsynaptic actin regulation and vesicle fusion; Red: Bind to actin or cadherins; Purple: ER to Golgi associated transport proteins; Beige: Cytoskeletal arrangement and neurite projection development; Teal green: Lamellipodia organization and regulating blood-brain barrier permeability, presence at the dendritic spine; Forest green: Endocytosis-related proteins and membrane organization.

Notably, the actin cytoskeletal remodelling protein Ras-related botulinum substrate 1 (RAC1) was detected, a protein detected in a yeast two-hybrid screen in unpublished results from our lab (*Ilie, A and Orlowski, J. unpublished data*) (Fig. 7C, green, center-left). Several other actin-associated proteins (e.g., α-actinin1/4, cortactin, integrin α3/β1, filamin-A/B/C, talin, vinculin and zyxin) critical for neurite development and synaptic function/plasticity were also biotinylated (Table 1) (114–119). Several proteins involved in endosomal trafficking also clustered together, including clathrin light chain A (CLTA), clathrin heavy chain (CLTC), spectrin β chain (SPTBN1), hepatocyte growth factor-regulated tyrosine kinase substrate (HGS), secretory carrier membrane protein 3 (SCAMP3), and the motor proteins kinesin-1 5B (KIF5B) and dynein cytoplasmic 1 heavy chain 1 (DYNC1H1). The clathrin subunits are known endocytic interactors, validating the approach (24). The identification of HGS, SCAMP3, KIF5B and DYNC1H1 represent putative novel interactors involved in NHE6 vesicle trafficking. HGS (a subunit of the endosomal sorting complex required for transport (ESCRT-0) complex) regulates endosomal sorting and plays a critical role in both recycling and degradation of membrane receptors (120). SCAMP3, which associates with HGS, has also been shown to promote endosomal receptor recycling and is enriched in vesicles containing TrkB/C receptors in cultured primary cortical neurons (121). Interestingly, SCAMP5 has recently been implicated in the trafficking of NHE6 to synaptic vesicles of rat hippocampal neurons (122). However, this finding remains uncertain because while we and others have localized NHE6 endosomes to a subset of presynaptic terminals in mouse hippocampal neurons, its presence in synaptic vesicles has not been generally detected by electron microscopy (81). Lastly, the motor proteins KIF5B (123–125) and DYNC1H1 (126) have been implicated in the membrane transport of select cargo along axons and dendrites. Significantly, conditional KO of *KIF5B* in mice impairs dendritic spine morphogenesis, synaptic plasticity and

memory formation (124). Similarly, *DYNC1H1* loss-of-function mutations cause a spectrum of neuropathologies, including intellectual disability, epilepsy, and motor dysfunction (126–131).

These preliminary findings identify interactions between NHE6, and proteins involved in endosomal trafficking, actin cytoskeletal remodeling, neuron development, maturation and function. Given the scope, we focused our attention on proteins directly involved in neurogenesis and the actin cytoskeleton (i.e., RAC1) and how this may impact vesicle trafficking.

TABLE 1: Gene Name and Description of NHE6 Proximate Interactome		
GENE	**DESCRIPTION**	**Total Unique Peptide Count $NHE6_{3F}$-APEX2**
ACTB	actin beta [Source:HGNC Symbol;Acc:HGNC:132]	13
ACTBL2	actin beta like 2 [Source:HGNC Symbol;Acc:HGNC:17780]	3
ACTN1	actinin alpha 1 [Source:HGNC Symbol;Acc:HGNC:163]	7
ACTN4	actinin alpha 4 [Source:HGNC Symbol;Acc:HGNC:166]	9
AFAP1	actin filament associated protein 1 [Source:HGNC Symbol;Acc:HGNC:24017]	2
AHNAK	AHNAK nucleoprotein [Source:HGNC Symbol;Acc:HGNC:347]	61
ALDOA	aldolase, fructose-bisphosphate A [Source:HGNC Symbol;Acc:HGNC:414]	3
ANXA11	annexin A11 [Source:HGNC Symbol;Acc:HGNC:535]	6
ANXA2	annexin A2 [Source:HGNC Symbol;Acc:HGNC:537]	15
ANXA6	annexin A6 [Source:HGNC Symbol;Acc:HGNC:544]	5
ANXA7	annexin A7 [Source:HGNC Symbol;Acc:HGNC:545]	2
CALD1	caldesmon 1 [Source:HGNC Symbol;Acc:HGNC:1441]	14
CALU	calumenin [Source:HGNC Symbol;Acc:HGNC:1458]	2
CAPRIN1	cell cycle associated protein 1 [Source:HGNC Symbol;Acc:HGNC:6743]	3
CFL1	cofilin 1 [Source:HGNC Symbol;Acc:HGNC:1874]	2
CLCC1	chloride channel CLIC like 1 [Source:HGNC Symbol;Acc:HGNC:29675]	2
CLTA	clathrin light chain A [Source:HGNC Symbol;Acc:HGNC:2090]	2
CLTC	clathrin heavy chain [Source:HGNC Symbol;Acc:HGNC:2092]	12
CNN2	calponin 2 [Source:HGNC Symbol;Acc:HGNC:2156]	4
CTNND1	catenin delta 1 [Source:HGNC Symbol;Acc:HGNC:2515]	3
CTTN	cortactin [Source:HGNC Symbol;Acc:HGNC:3338]	8
DBNL	drebrin like [Source:HGNC Symbol;Acc:HGNC:2696]	3
DPYSL2	dihydropyrimidinase like 2 [Source:HGNC Symbol;Acc:HGNC:3014]	2
DPYSL3	dihydropyrimidinase like 3 [Source:HGNC Symbol;Acc:HGNC:3015]	3
DYNC1H1	dynein cytoplasmic 1 heavy chain 1 [Source:HGNC Symbol;Acc:HGNC:2961]	6
EZR	ezrin [Source:HGNC Symbol;Acc:HGNC:12691]	5
FLNA	filamin A [Source:HGNC Symbol;Acc:HGNC:3754]	82
FLNB	filamin B [Source:HGNC Symbol;Acc:HGNC:3755]	50
FLNC	filamin C [Source:HGNC Symbol;Acc:HGNC:3756]	39

HGS	hepatocyte growth factor-regulated tyrosine kinase substrate [Source:HGNC Symbol;Acc:HGNC:4897]	3
ITGA3	integrin subunit alpha 3 [Source:HGNC Symbol;Acc:HGNC:6139]	2
ITGB1	integrin subunit beta 1 [Source:HGNC Symbol;Acc:HGNC:6153]	6
KIF5B	kinesin family member 5B [Source:HGNC Symbol;Acc:HGNC:6324]	6
KTN1	kinectin 1 [Source:HGNC Symbol;Acc:HGNC:6467]	14
LASP1	LIM and SH3 protein 1 [Source:HGNC Symbol;Acc:HGNC:6513]	4
LMNA	lamin A/C [Source:HGNC Symbol;Acc:HGNC:6636]	7
MAP1B	microtubule associated protein 1B [Source:HGNC Symbol;Acc:HGNC:6836]	34
MAP4	microtubule associated protein 4 [Source:HGNC Symbol;Acc:HGNC:6862]	11
NES	nestin [Source:HGNC Symbol;Acc:HGNC:7756]	2
PDLIM5	PDZ and LIM domain 5 [Source:HGNC Symbol;Acc:HGNC:17468]	3
PLEC	plectin [Source:HGNC Symbol;Acc:HGNC:9069]	29
RAC1	Rac family small GTPase 1 [Source:HGNC Symbol;Acc:HGNC:9801]	2
SCAMP3	secretory carrier membrane protein 3 [Source:HGNC Symbol;Acc:HGNC:10565]	2
SEC23IP	SEC23 interacting protein [Source:HGNC Symbol;Acc:HGNC:17018]	2
SEC24C	SEC24 homolog C, COPII coat complex component [Source:HGNC Symbol;Acc:HGNC:10705]	3
SEC31A	SEC31 homolog A, COPII coat complex component [Source:HGNC Symbol;Acc:HGNC:17052]	3
SH3PXD2B	SH3 and PX domains 2B [Source:HGNC Symbol;Acc:HGNC:29242]	2
SLC9A6	solute carrier family 9 member A6 [Source:HGNC Symbol;Acc:HGNC:11079]	3
SPTAN1	spectrin alpha, non-erythrocytic 1 [Source:HGNC Symbol;Acc:HGNC:11273]	12
SPTBN1	spectrin beta, non-erythrocytic 1 [Source:HGNC Symbol;Acc:HGNC:11275]	5
SYNPO2	synaptopodin 2 [Source:HGNC Symbol;Acc:HGNC:17732]	19
TJP1	tight junction protein 1 [Source:HGNC Symbol;Acc:HGNC:11827]	3
TJP2	tight junction protein 2 [Source:HGNC Symbol;Acc:HGNC:11828]	11
TLN1	talin 1 [Source:HGNC Symbol;Acc:HGNC:11845]	6

TNKS1BP1	tankyrase 1 binding protein 1 [Source:HGNC Symbol;Acc:HGNC:19081]	5
TPM3	tropomyosin 3 [Source:HGNC Symbol;Acc:HGNC:12012]	6
TPM4	tropomyosin 4 [Source:HGNC Symbol;Acc:HGNC:12013]	7
TUBA1A	tubulin alpha 1a [Source:HGNC Symbol;Acc:HGNC:20766]	15
TUBA4A	tubulin alpha 4a [Source:HGNC Symbol;Acc:HGNC:12407]	9
TUBB	tubulin beta class I [Source:HGNC Symbol;Acc:HGNC:20778]	10
TUBB4B	tubulin beta 4B class IVb [Source:HGNC Symbol;Acc:HGNC:20771]	7
VCL	vinculin [Source:HGNC Symbol;Acc:HGNC:12665]	14
VIM	vimentin [Source:HGNC Symbol;Acc:HGNC:12692]	41
YWHAQ	tyrosine 3-monooxygenase/tryptophan 5-monooxygenase activation protein theta [Source:HGNC Symbol;Acc:HGNC:12854]	4
YWHAZ	tyrosine 3-monooxygenase/tryptophan 5-monooxygenase activation protein zeta [Source:HGNC Symbol;Acc:HGNC:12855]	2
ZYX	zyxin [Source:HGNC Symbol;Acc:HGNC:13200]	6

Table 1 NHE6 interacting proteome as determined by APEX2

Columns: Left: Gene name for detected protein; Center: Description/full name of protein; Right: Peptide counts detected by Thermo Scientific Orbitrap Fusion™ Mass Spectrometer for corresponding protein.

3.3 NHE6 and RAC1 co-immunoprecipitate in AP-1 cells

To confirm an interaction (direct or indirect) between NHE6 and RAC1, a co-immunoprecipitation (co-IP) assay was performed (132–134). This protein (RAC1) has been implicated in a diverse array of cellular functions, including actin cytoskeletal reorganization, cell spreading and cell adhesion, and neurogenesis (135,136). Because RAC1 exists *in vivo* in either an inactive (RAC1-GDP) or active (RAC1-GTP) state, we assessed which of these forms bound to NHE6. To this end, we used MYC-tagged wild-type RAC1 ($_{MYC}$RAC1-WT), a dominant negative (DN) inactive form, $_{MYC}$RAC1-T17N, which forms a tight complex with a guanine nucleotide exchange factor (GEF) that prevents the GEF from activating RAC1, and a constitutively active (CA) form, RAC1-Q61L, incapable of GTP hydrolysis (136,137).

To co-IP RAC1 and NHE6, AP-1 cells stably expressing HA-tagged NHE6 (NHE6$_{HA}$) were transfected with $_{MYC}$RAC1-WT, $_{MYC}$RAC1-T17N, $_{MYC}$RAC1-Q61L DNA or empty vector pCMV as a negative control. As shown in Figure 8, $_{MYC}$RAC1-WT and $_{MYC}$RAC1-Q61L, but not $_{MYC}$RAC1-T17N were present in immunoprecipitated NHE6$_{HA}$ complexes, with the strongest signal generated by the constitutively active $_{MYC}$RAC1-Q61L.

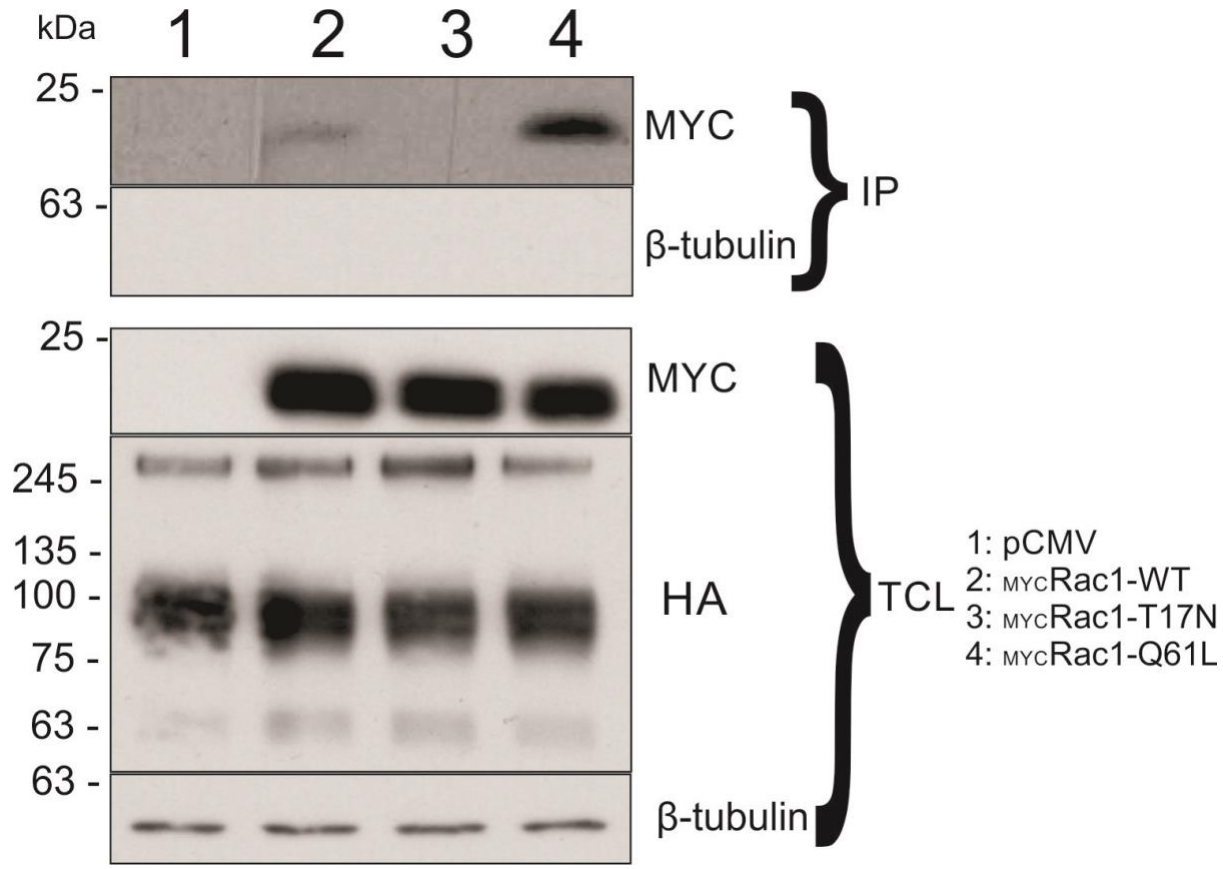

Figure 8 Co-Immunoprecipitation of RAC1 with NHE6

Co-immunoprecipitation (co-IP) blot along with total transfected cell lysates using a monoclonal MYC antibody for pCMV, $_{MYC}$RAC1-WT, $_{MYC}$RAC1-T17N, and $_{MYC}$RAC1-Q61L in NHE6$_{HA}$ stably expressing AP-1 cells. AP-1 cells stably expressing NHE6$_{HA}$ were grown in 10-cm dishes and transfected with 5 µg pCMV, $_{MYC}$RAC1-WT, $_{MYC}$RAC1-T17N, and $_{MYC}$RAC1-Q61L DNA. Cells were lysed at 24 h post-transfection. Precleared cell lysates were immunoprecipitated with rabbit anti-HA antibody and probed for MYC by western blotting. The top panel shows $_{MYC}$RAC1 expression in complexes pulled down with NHE6. The same membrane was stripped and subsequently blotted for β-tubulin, serving as a negative control, since tubulin does not immunoprecipitate with anti-HA. The bottom 3 panels show total cell lysates (TCL) blotted for NHE6$_{HA}$ and $_{MYC}$RAC1, as well as β-tubulin as a loading control (lower blots). This experiment was carried out in three separate trials.

3.4 *In vitro* Glutathione-S-transferase pull-down assays between NHE6 and RAC1

To further characterize the site of interaction between NHE6 and RAC1, *in vitro* pull-down assays were performed by incubating glutathione S-transferase (GST) fusions of sequentially overlapping segments of the NHE6 C-terminus (a.a. 531-701) with AP-1 cell lysates expressing the various RAC1 constructs (schematic in Fig. 9A) (138,139). pGEX-2t alone was used as a negative control. The isolated complexes were immunoblotted for MYC to detect RAC1. When using AP-1 cells transiently transfected with $_{MYC}$RAC1-WT, a complex between the two proteins was detected with the full-length NHE6 C-terminus (amino acids 531-701) (Lane 6 in Figure 9B). The interaction complex was also obtained with each NHE6 fragment except for the one encompassing amino acids 531-558 (Fig. 9B). These data indicate that amino acids 558-596 are sufficient to confer binding to RAC1. It was noted that the longer fragment corresponding to amino acids 531-653 exhibited less binding to RAC1 compared to amino acids 558-596. While the reason for this is uncertain, we speculate this slightly longer fragment may adopt an aberrant conformation that reduces the binding affinity. Alternatively (and more likely), this is the lane with the lowest amount of GST fusion protein, as seen in the respective Ponceau blot. A similar pattern can be observed with the constitutively active $_{MYC}$RAC1-Q61L, in addition to binding to all fusion proteins, including the first fragment, although more intense binding is observed (Fig. 9D). By contrast, weak binding of the dominant-negative $_{MYC}$RAC1-T17N mutant was observed only with the full-length C-tail (Fig. 9C). These *in vitro* binding data are consistent with the results obtained by the co-IP experiments.

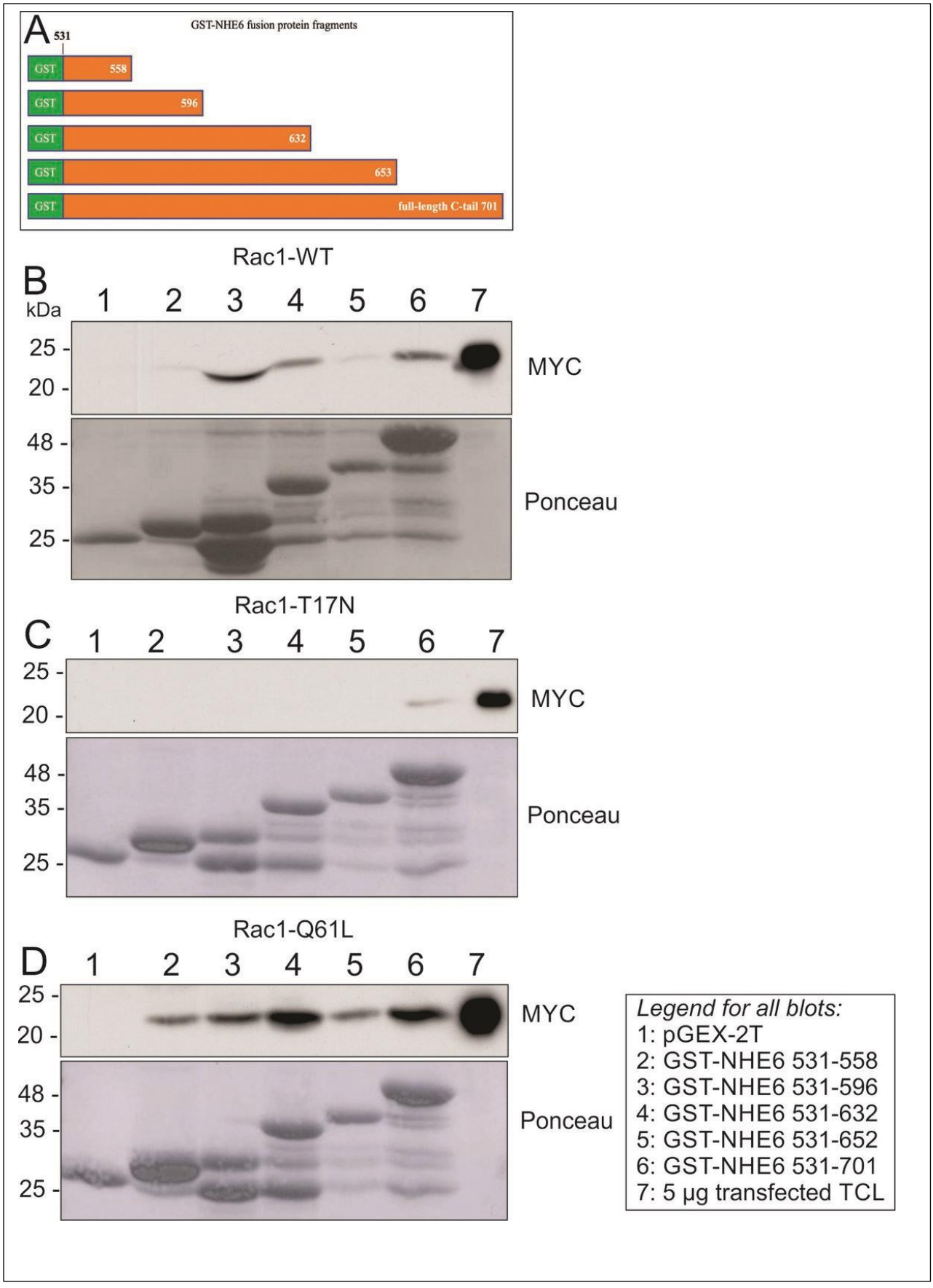
A
GST-NHE6 fusion protein fragments
531
GST
558
GST
596
GST
632
GST
653
GST
full-length C-tail 701
Rac1-WT
B
kDa
1 2 3 4 5 6 7
25 -
20 -
MYC
48 -
35 -
25 -
Ponceau
Rac1-T17N
C
1 2 3 4 5 6 7
25 -
20 -
MYC
48 -
35 -
25 -
Ponceau
Rac1-Q61L
D
1 2 3 4 5 6 7
25 -
20 -
MYC
48 -
35 -
25 -
Ponceau
Legend for all blots:
1: pGEX-2T
2: GST-NHE6 531-558
3: GST-NHE6 531-596
4: GST-NHE6 531-632
5: GST-NHE6 531-652
6: GST-NHE6 531-701
7: 5 µg transfected TCL

Figure 9 *In vitro* GST pulldown assay between Wild-type RAC1 and NHE6 C-terminal tail
(A) Schematic representation of GST-NHE6 C-terminal fusion proteins. (B-D) AP-1 cell lysates were incubated with Glutathione Sepharose^{TM} beads coated with either GST alone (pGEX-2t condition) or GST fused with overlapping fragments of the NHE6 C-terminal tail. Pulled-down proteins were immunoblotted for MYC-tagged RAC1 (top) to detect WT, T17N, and Q61L mutants, respectively. Expression of GST fusion proteins was visualized by Ponceau staining (bottom). These data are representative of 3 independent experiments.

3.5 Colocalization of NHE6 and RAC1 in AP-1 cells

The interaction between NHE6 and RAC1 in AP-1 cells was further examined visually by immunofluorescence confocal microscopy. Cells examined include AP-1 cells stably expressing $NHE6_{HA}$ alone, AP-1 cells transiently transfected (24 h) with either $_{MYC}$Rac1-WT, $_{MYC}$Rac1-T17N and $_{MYC}$Rac1-Q61L alone, and AP-1 cells stably expressing $NHE6_{HA}$ and transiently cotransfected (24 h) with $_{MYC}$Rac1-WT, $_{MYC}$Rac1-T17N and $_{MYC}$Rac1-Q61L.

In AP-1 cells stably expressing $NHE6_{HA}$, the bulk of the transporter localized to recycling endosomes in the perinuclear/pericentriolar region, with a nominal amount marginally visible at the cell surface (Figure 10A), consistent with previous reports (96,140). In AP-1 cells devoid of exogenous $NHE6_{HA}$, the distribution of transiently transfected $_{MYC}$RAC1 varied according to its state of activation. $_{MYC}$RAC1-WT displayed a punctate distribution that was dispersed along or near the plasma membrane as well as intracellularly (Fig. 10A). The internal location is consistent with RAC1 binding to endosomes (141,142) and/or sequestration from membranes by binding to Rho-GTPase guanine nucleotide dissociation inhibitors (RhoGDIs) (143,144). Dominant-negative $_{MYC}$RAC1-T17N also appears to show a diffuse distribution (both plasma membrane and cytosol) whereas constitutively active $_{MYC}$RAC1-Q61L accumulated preferentially at the plasma membrane and membrane ruffles and to a lesser extent in the cytosol, findings consistent with earlier observations (Fig. 10A) (145,146). Morphologically, $_{MYC}$RAC1-WT did not induce noticeable changes in gross cell size compared to parental cells, whereas $_{MYC}$RAC1-T17N and $_{MYC}$RAC1-Q61L caused cell contraction and expansion, respectively, as documented previously (145). Intriguingly, in the presence of $NHE6_{HA}$, $_{MYC}$RAC1-WT exhibited increased accumulation at the cell surface in a non-contiguous pattern that largely overlapped that of surface $NHE6_{HA}$ (Fig. 10B). The co-occurrence of both proteins was dramatically enhanced with the constitutively active

MYCRAC1-Q61L, not only at the plasma membrane but also in endosomes concentrated in the perinuclear/pericentriolar region. Notably, both proteins accumulated at the leading edge of migrating AP-1 cells (Figure 10B), suggesting a role for NHE6-RAC1-containing endosomes in polarized delivery of cargo important for actin cytoskeletal remodeling and directed cell migration. Consistent with this notion, NHE6 has been implicated in the polarized delivery of membrane lipids and proteins to the apical membrane of HepG2 liver cells (147). Likewise, a gradient of activated RAC1 can be visualized in migrating fibroblasts with the highest concentrations at the leading edge (148). By contrast, MYCRAC1-T17N showed very little visual overlap with MYCRAC1-WT.

To quantify the degree of colocalization between vesicles containing NHE6 and RAC1 in AP-1 cells, Manders' colocalization coefficients (MCC) were calculated for both markers. With respect to the WT and DN mutants, The MCC for RAC1 with NHE6 were approximately 0.30 and 0.25, meaning 30% and 25% of RAC1-positive pixels were also positive for NHE6, respectively (Fig. 10C, D). However, the MCC for RAC1's CA form was 0.53, meaning 53% of RAC1-positive pixels were positive for NHE6 (Fig. 10E). These values indicate that the CA form of RAC1 is moderately colocalized with NHE6 in AP-1 cells, and less for the WT and DN forms. Some colocalization of RAC1 WT and NHE6 can be observed at the plasma membrane (Figure 10B). This is consistent with what was observed with the co-IP data, where a strong complex with RAC1's CA form is present with NHE6.

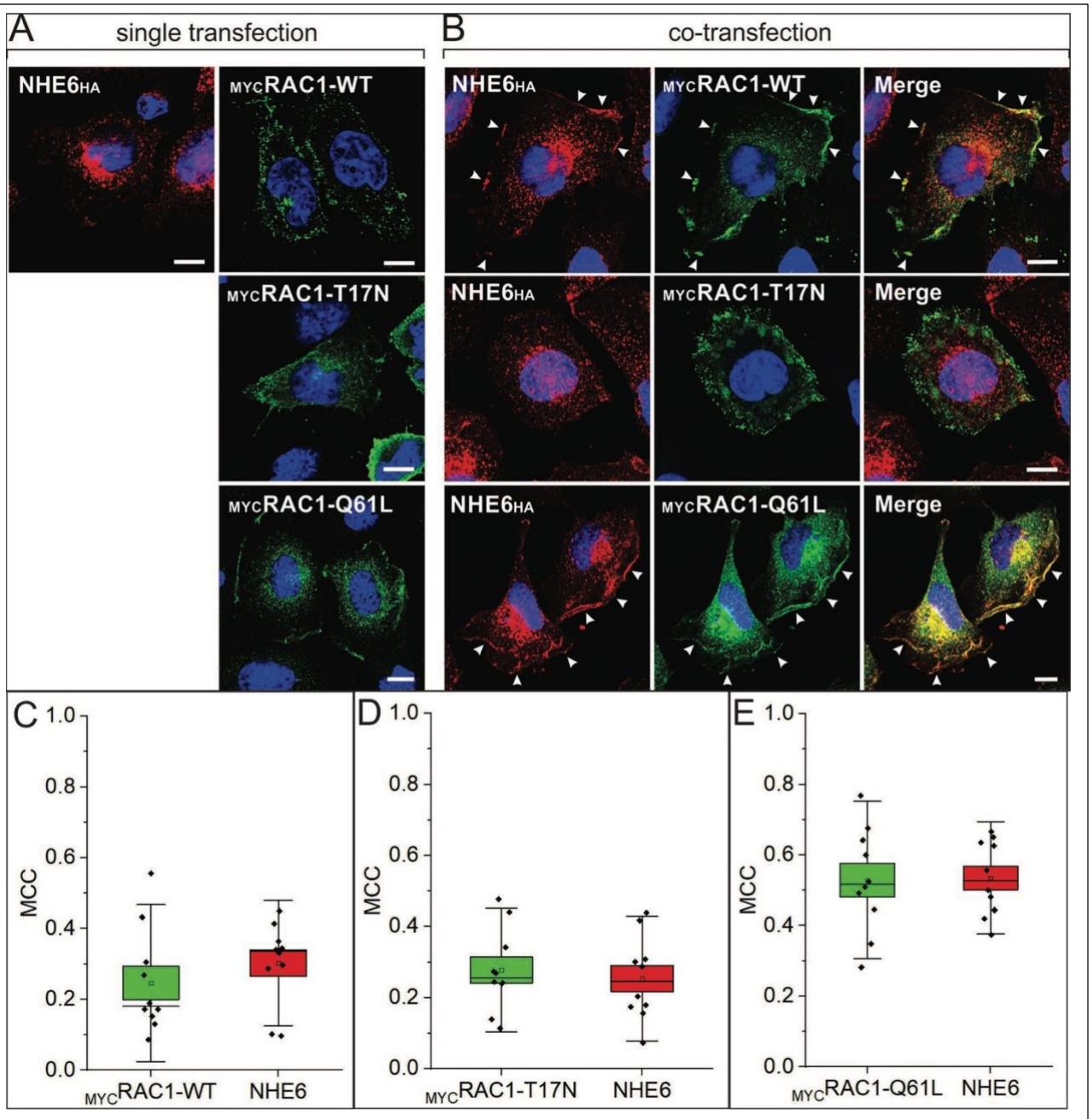

Figure 10 Co-Localization Analysis of NHE6 and RAC1 in AP-1 cells

(A) Single transfections of AP-1 cells stably expressing $NHE6_{HA}$ alone or AP-1 cells transiently transfected (24 h) with either wildtype $_{MYC}$Rac1, $_{MYC}$Rac1-T17N and $_{MYC}$Rac1-Q61L alone. (B) AP-1 cells stably expressing $NHE6_{HA}$ and transiently cotransfected (24 h) with $_{MYC}$Rac1, $_{MYC}$Rac1-T17N and $_{MYC}$Rac1-Q61L. Scales all represent 10 nm. (C-E) Manders' colocalization coefficients were calculated using ImageJ analysis software for MYC with NHE6 in individual cells from (B). Box plots display the standard error of the mean (SEM) and error bars represent the standard deviation (SD), and the individual data points from each cell are shown. 10 cells were analyzed from each population.

3.6 Cell Surface Biotinylation Analysis of NHE6 and RAC1 interaction

To further evaluate the colocalization of NHE6 and RAC1 at the plasma membrane, we performed a cell surface biotinylation assay (149). To accomplish this, MYC-tagged RAC1 constructs were transiently transfected into AP-1 cells and AP-1/NHE6$_{HA}$ stable cells. Twenty-four hours post-transfection, the cells were placed on ice to stop endocytosis, then biotin was added and subsequently washed, and the cells were lysed. Immunoblots were probed with HA or MYC to detect NHE6 or RAC1, respectively. In both cell lines, active RAC1 (i.e., wild-type and constitutively active) were detected at the cell surface (Fig. 11). The dominant-negative $_{MYC}$RAC1-T17N was detected at the cell surface in NHE6 stable cell lines but in considerably lower amounts relative to its wild-type or constitutively active counterparts. It appears that trafficking of NHE6 to the plasma membrane is not markedly affected by RAC1, since similar levels of plasmalemmal NHE6 can be observed in lanes 6-8, corresponding to the different transfected $_{MYC}$RAC1 constructs. On the contrary, RAC1 trafficking to the surface is increased in the presence of NHE6, as observed in Figure 11, speculating that NHE6 plays a role in RAC1's trafficking.

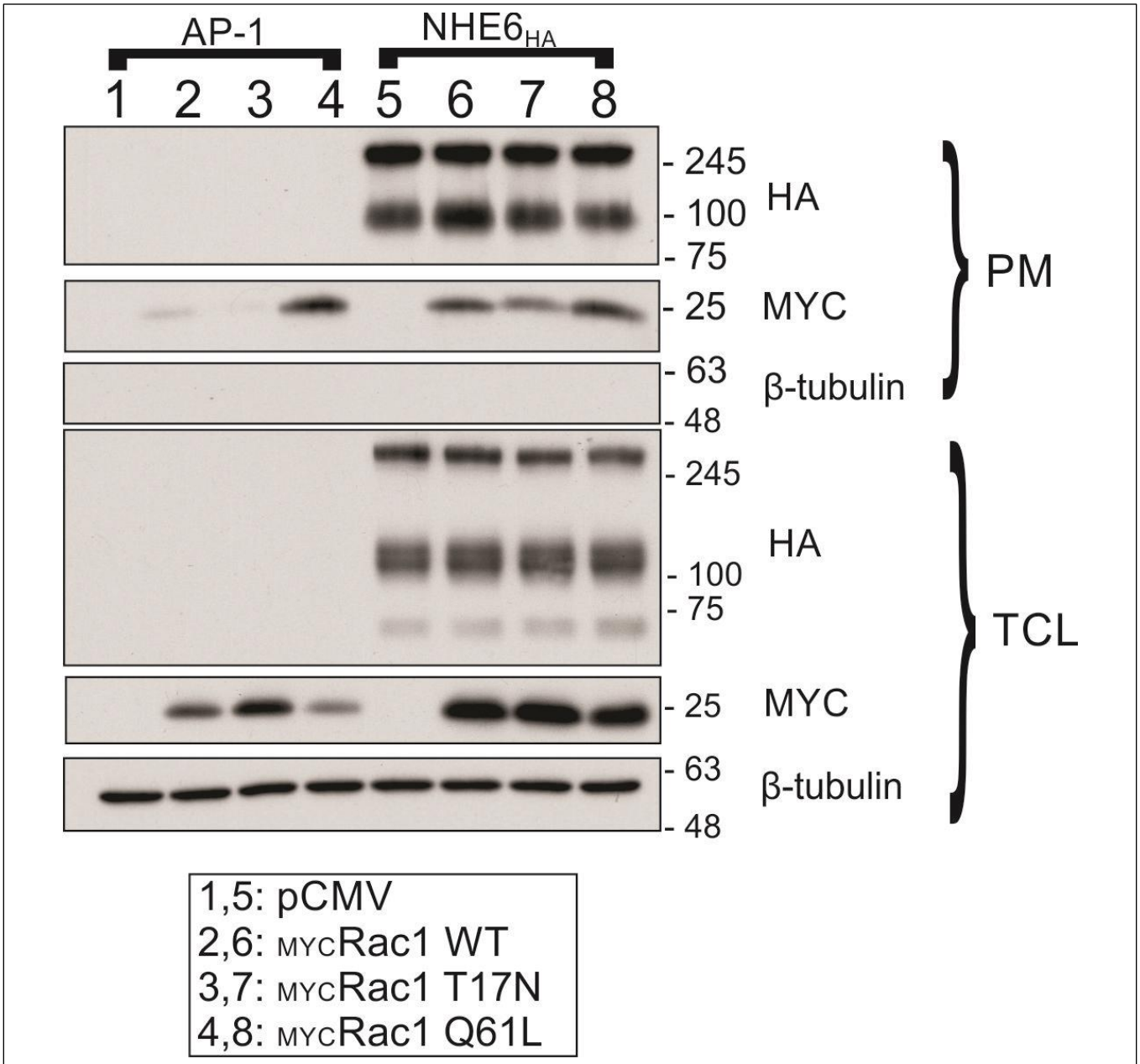

Figure 11 Cell Surface Biotinylation Analysis of NHE6 and RAC1 interaction
AP-1 cells (stabling expressing NHE6 or not) were grown to confluency and used directly or transfected with pCMV and MYC-tagged RAC1 constructs. Plasma membrane (PM) proteins were labeled with biotin as described in 'Materials and Methods'. Total cell lysates (TCL) were prepared and a portion representing the total fraction was removed. The remaining supernatant was incubated with NeutrAvidin® Agarose beads to extract the biotinylated cell surface proteins. For total cell lysates, aliquots representing ~1.75% (20 µg protein) of the original lysates of non-transfected AP-1 cells or $NHE6_{HA}$-transfectants were examined by SDS–PAGE. For the cell surface fractions, 50% and 100% of the entire biotinylated proteins extracted from total lysates of non-transfected AP-1 cells or $NHE6_{HA}$-transfectants, respectively, were examined by SDS–PAGE. The immunoblots were probed with mouse monoclonal anti-HA and anti-MYC antibodies to detect NHE6 and RAC1 (upper panels) and a monoclonal anti-beta-tubulin antibody (lower panels). These data are representative of 3 independent experiments.

DISCUSSION

NHE6 is known to modulate pH homeostasis, trafficking and signalling of recycling endosomes in neurons as well as other cell types, yet exactly how this occurs remains largely unknown. To investigate the underlying molecular mechanisms, proximity biotin-labelling identification (BioID) methodology was used to define the human NHE6 proximate proteome in SH-SY5Y cells, a well-defined neuronal model system. This analysis yielded 66 proteins that clustered into several related biological processes involved in neuronal morphogenesis and differentiation, including synapse organization, actin cytoskeletal organization and organelle localization.

The most abundant proteins related to “cytoskeleton organization”. These included annexins (ANXA), filamins (FLMA/B/C), tubulins (TUBA/B), vimentin (VIM), actins (ACTB) and actinins (ACTN), etc. Annexins are documented to play many important roles such as the structural organization of the cell, factors important for guiding intracellular signaling and growth regulation, suggesting that NHE6 may play potential roles in these processes (150,151). Members of the tubulin family were also detected, although this could be expected since vesicles of the endosomal pathway, including those which carry NHE6, regularly traffic along microtubules (152). All three isoforms of filamins, which act as actin cross-linkers, were also detected and have been demonstrated to regulate postsynaptic membrane architecture in *Drosophila melanogaster* species (153,154).

Another overlapping set of categories included cell morphogenesis, neuron differentiation and cell projection organization. Proteins known to be associated with the latter categories include cortactin (CTTN) and caldesmon 1 (CALD1). The main role of CTTN is to encourage the development of branching actin networks (115). Numerous studies have demonstrated that cortactin interacts with the actin-related protein-2/3 (Arp2/3) complex via its N-terminal acidic

(NTA) domain and that this contact facilitates actin nucleation, supporting cortactin's nucleation promotion factor function (155,156). At the cell periphery, cortactin, Arp2/3, and filamentous actin (F-actin) interact to cause the production of branched actin, which facilitates migration and invasion (156). Concurrently, CALD1 is known to regulate actomyosin contraction, actin filament dynamics and cytoskeleton remodeling in smooth muscle and nonmuscle cells (157). An interaction between CTTN and CALD1 has been previously identified through pulldown and ELISA-related methods, suggesting that actin filament formation and stability in non-muscle cells may be further influenced by the interaction between CTTN and CALD1 (158). It is reasonable to speculate that because they were detected through BioID as either interacting or near NHE6, the exchanger may play a role in either cell migration and formation of lamellipodia or as a link in the trafficking of these proteins to their associative complex.

More proteins linked to cytoskeletal arrangement and neurite projection development include microtubule-associated proteins (MAPs), whose main function is to act as cross-linkers between actin filaments and microtubules (159). The detection of these proteins further enhances the notion that NHE6 is associated with the generation of polarized cytoskeletal structures. Specifically, MAPs 1B and 4 were detected. MAP1B is regulated through phosphorylation events and influences microtubule stability, microfilaments and motility of the neuronal growth cone in neurons (160). Mice harboring mutations in *MAP1B* leading to the formation of a deficient protein exhibit impaired long-term potentiation (LTP) within hippocampal neurons, posing a curiosity towards a potential link with NHE6's involvement in LTP (81,161). Evidence of MAP4 associating with dendritic microtubules is present, with research suggesting that the cytoskeletal-related protein plays a role in the dynamic reorganization of dendritic spines (162).

Another important protein related to the cytoskeleton, but also organelle localization and endocytosis, is RAC1. RAC1 is a member of the Rho family of small GTPases that play central roles in actin cytoskeletal remodelling, vesicle trafficking and neuronal morphogenesis (146,163,164). It also plays a role in development, as ablation of RAC1 results in embryonic lethality in mice (165). In neurons, they control a myriad of processes, including neurite (axons, dendrites) growth and differentiation, membrane ruffling, as well as the development, maintenance, and plasticity of dendritic spines (166). RAC1 and other Rho GTPases are known to transit through various types of early and recycling endosomes as a means to control cytoskeletal remodelling at discrete subcellular locations, including dendritic spines and their maturation (163,167–169). An example of this would be RAC1's direct effect on F-actin assembly during chemotaxis, as inactive RAC1 (using a dominant negative mutant) completely abrogates cell migration in both mammalian and non-mammalian cell models (170,171). Because of RAC1's effects on cell migration and differentiation, mutations leading to the constitutively active state of RAC1 have been implicated in tumors and metastases (172,173). We propose NHE6 encounters RAC1 and helps promote its localization into dendritic spines, thus promoting proper spine maturation. This is supported by our cell surface biotinylation study, where RAC1's presence at the cell surface was increased in the presence of NHE6 (Figure 11).

To better explain our hypothesis, it is necessary to describe the signaling cascade of RAC1. Under basal conditions, cytoplasmic RAC1 is tightly bound to Rho GDP-dissociation inhibitor (RhoGDI) (174). Being a GTPase, RAC1 is activated by guanine nucleotide exchange factors (GEFs) and inactivated by GTPase-activating proteins (GAPs). Some of the GEFs known to activate RAC1 include T-lymphoma invasion and metastasis gene 1 (Tiam1), 5-trisphosphate-dependent Rac exchange factor 1 (P-Rex1), and neuron-specific kalirin-7, with reports showing

that they can also act as scaffolding proteins (175,176). It is previously proposed that only once RAC1 is translocated to the plasma membrane that the RhoGDI is dissociated, allowing for RAC1 to interact with GEFs for its activation. Ca^{2+}/calmodulin-dependent protein kinase II (CaMKII) recruits some of these GEFs listed above and triggers LTP (177,178). Based on our data, we hypothesize that NHE6 interacts with RAC1 on endosomes which may facilitate its activation and delivery to the plasma membrane of dendritic spines.

RAC1 acts on actin-binding proteins (such as ACTN), which play a central role in spine formation, synapse formation/removal, and synaptic plasticity (179,180). Cofilin (CFL), another protein detected in our BioID analysis, is an actin-inactivating factor, cleaving F-actin at its tips which prevents spine growth and maturation (181,182). Through RAC1-mediated activation of p21-activated kinase 1 (PAK1) and LIM-kinase 1 (LIM-K1), CFL becomes phosphorylated and inactive, thereby allowing actin polymerization and spine maturation to proceed (182,183).

Since RAC1 is involved in cytoskeletal reorganization and necessary for both spine growth and stabilization, we can speculate that similar mechanisms may also play a role in the morphology of NHE6-altered neurons. Rab7, an established LE marker controlling late endocytic trafficking, directly interacts with RAC1 and both proteins colocalize in endosomes at the perinuclear region and on vesicles near the plasma membrane (184). Rab7, which activates RAC1, promotes its re-localization to the plasma membrane, more specifically to the leading edge to stimulate cell migration, in association with vimentin, another protein detected in our analysis (184). Furthermore, Rab7 is involved in the proper axonal transport of neurotrophin signalling, notably in the BDNF/TrkB signaling cascade, which is involved in the proper development of dendritic spines (185). We speculate that this can be attributed to NHE6's interaction with RAC1, an event that we propose is necessary for the proper growth of dendritic spines.

Neuronal plasticity has been suggested to require proteins involved in cytoskeleton reorganization and actin polymerization (169), and dendritic spine morphology has been widely suggested to be involved in proper learning and aging (186). Thus, we believe that NHE6 may present a link between proper neuronal circuitry for learning and memory and the actin cytoskeleton in hippocampal neurons. Rho GTPases have also been found to interact with other NHEs (187). RhoA has been implicated in the regulation of NHE3 at the apical membranes of epithelial cells of the kidney and gastrointestinal tract, although evidence for a direct interaction is lacking (187). To confirm that full-length NHE6 and RAC1 interact *in vitro,* we first performed co-immunoprecipitation experiments using CHO AP-1 cells stably expressing NHE6 and transiently co-transfected with RAC1-WT, constitutively active RAC1-Q61L and dominant negative inactive RAC1-T17N. Both RAC1-WT and RAC1-Q61L formed a complex with NHE6, with the latter forming a more robust association. By contrast, RAC1-T17N failed to form a stable complex (Figure 8). This suggests that NHE6 preferentially interacts with active RAC1. This finding was corroborated by the imaging data presented in Fig. 10B, D. Collectively, this suggests that NHE6 facilitates, at least in part, the endosomal delivery of active RAC1 to the plasma membrane where it can regulate the actin cytoskeleton to promote the polarized formation of lamellipodia at the leading edge and directed cell migration.

Furthermore, a role for NHE6 in polarized delivery of cargo to the plasma membrane has been documented in hepatoma G2 (HepG2) cells. NHE6 was found to control the transcytosis of bulk membrane lipids from the basal to apical surface (147). Altered NHE6 expression in these cells resulted in less efficient retention of bulk membrane and bile canalicular proteins (e.g. dipeptidyl peptidase IV) at the apical membrane (147).

The distribution of lipids has a significant impact on the recruitment of RAC1 effectors to the membrane. Lipids containing cholesterol- and sphingolipid-enriched domains localize to different membrane domains at the plasma membrane and in endosomal compartments (23). This helps to attract certain effectors that not only create signalling platforms but also regulate membrane dynamics. While controlling endocytic transport, RAC1 activity is regulated by Arf6 for endocytic trafficking and recycling to and from the cell surface (23,188). In addition to verifying the NHE6 and RAC1 interaction in cell model systems, we performed GST pulldown assays to identify the region of the NHE6 C-terminal tail that interacts with RAC1. We showed that amino acids 558-596 of NHE6 seem to be important for RAC1 binding since the NHE6/RAC1 interaction is abolished when the C-terminal tail is truncated before these residues (Figure 9B). While these results are promising, further mutagenesis studies of that site are warranted to verify the NHE6/RAC1 interaction.

While we cannot rule out the possibility of another protein being present in NHE6/RAC1 interaction complex, it is likely that NHE6 and RAC1 are interacting (or in part very closely interacting) partners since the constitutively active form of RAC1 (Q61L) displayed strong colocalization with NHE6 (53%), as determined by Manders Colocalization Coefficient (MCC). Previous unpublished yeast two-hybrid screening studies from our lab also identified RAC1 as a direct interactor of NHE6 (*Ilie, A. and Orlowski, J., unpublished data*). Although RAC1's CA form exhibited substantial co-localization, its WT form did not exhibit the same degree of co-localization. However, this is not unexpected, as WT RAC1 exists in both inactive and active states. WT RAC1 exhibited some co-localization at the cell surface (Fig. 10B), speculating that NHE6 and its active form are working together.

Since RAC1 interacts with the NHE6 C-terminal tail, as determined through the GST pulldown assay, we hypothesized that either protein may be important for their respective trafficking to the plasma membrane. To examine this, a cell surface biotinylation assay was performed. Our preliminary data from these experiments performed in AP-1 cells indicated that RAC1, in either its WT, DN or CA forms, did not affect NHE6's trafficking to the cell surface. On the contrary, the presence of NHE6 appeared to increase all the forms of RAC1 at the cell surface (Figure 11). In the absence of NHE6, lower expression of WT and DN RAC1 was detected at the cell surface. By contrast, the cell surface expression of the CA mutant remained consistent regardless of the presence or absence of NHE6. Future work includes performing alanine-scanning or site-directed mutagenesis of the RAC1 binding site to test the effect of the NHE6 mutant on neuronal morphology and function. In this regard, a CS patient possesses an NHE6 mutation located within the binding site of RAC1 (unpublished observation). Whether this mutation disrupts the NHE6-RAC1 interaction remains to be determined.

Collectively, these initial findings suggest that NHE6 may interact spatially and temporally with RAC1 to form part of a novel mobile signalling complex involved in recycling endosomal trafficking and actin remodelling in dendritic spines, which we hypothesize is important for optimal synapse morphology and plasticity (Figure 12).

Aside from RAC1, previous studies have identified other direct interactors of NHE6 that may play key roles in its regulation (189,190). RACK1 (receptor for activated C kinase 1), a scaffolding protein localizing to the cytoplasm, forms a protein complex with NHE6, among other NHEs *in vivo* (189). Microscopic analyses revealed that RACK1 partially colocalizes with NHE6, further suggesting an interaction (189). Knockdown of the scaffolding protein in HeLa cells resulted in the alkalinization of endosomes and reduced plasma membrane levels of NHE6, suggesting that

the disruption of the RACK1/NHE6 interaction is important in regulating NHE6's function for regulating endosomal pH as well as its cellular distribution (189).

A second direct interacting protein identified with NHE6 is AT2 (angiotensin II subtype receptor AT2), a vasoconstrictor and sodium homeostasis regulator (191). Because a link between angiotensin II and NHEs has already been discovered in smooth muscle cells and myocytes through the downstream signalling (192–194), its role in regulating NHE6 by direct interaction was further investigated. Yeast two-hybrid analysis using AT2 as the bait protein identified NHE6 as a direct interactor (190). It was revealed that a region comprising of the fifth intracellular loop and the beginning of the C-terminal portion of NHE6 was identified to bind AT2 upon AT2's activation by angiotensin II, suggesting roles for AT2-mediated signaling events (190).

It is important to note that one of the shortcomings of our current BioID approach is that it is semi-quantitative and requires higher peptide counts to distinguish potential candidates from background and thus may miss low-abundance proteins that are nevertheless biologically important. To generate a higher confidence list of candidates, we can couple proximity-labelling with quantitative MS using metabolic labelling, such as "Stable Isotope Labelling by Amino acid in Cell culture" (SILAC) (97). Alternatively, quantitative MS can be done with "isobaric Tags for Relative and Absolute Quantification" (iTRAQ) and "Tandem Mass Tags" (TMT) (97). However, these analyses are more complex and more expensive, which precludes easy adoption.

In summary, our results provide additional insight into the molecular mechanisms by which NHE6, whose mutations are linked to CS, impair recycling endosomal pH homeostasis and cargo trafficking, and ultimately cell function and survival. The APEX2 method is one of the latest methods of BioID used for identifying proteins within a target protein's proximity. We have defined the molecular network of NHE6 revealing a potential new gateway into investigating the

interacting partners of NHE6, opening a new spectrum into the understanding of the exchanger. The list of interacting proteins detected by this method, although preliminary, will guide future investigations to delineate the molecular network of proteins that interact with NHE6 and how its mutations lead to CS while investigating NHE6's influence on receptor trafficking and synaptic plasticity, as we have begun to investigate with RAC1. NHE6 may play a crucial role as a signalling scaffold for RAC1 in the vesicular trafficking of cargo, signaling and cytoskeletal reorganization in live cells. Such knowledge has the potential to identify novel diagnostic and treatment options for CS that may also apply to other disorders showing deficits in actin cytoskeletal organization and cell signalling.

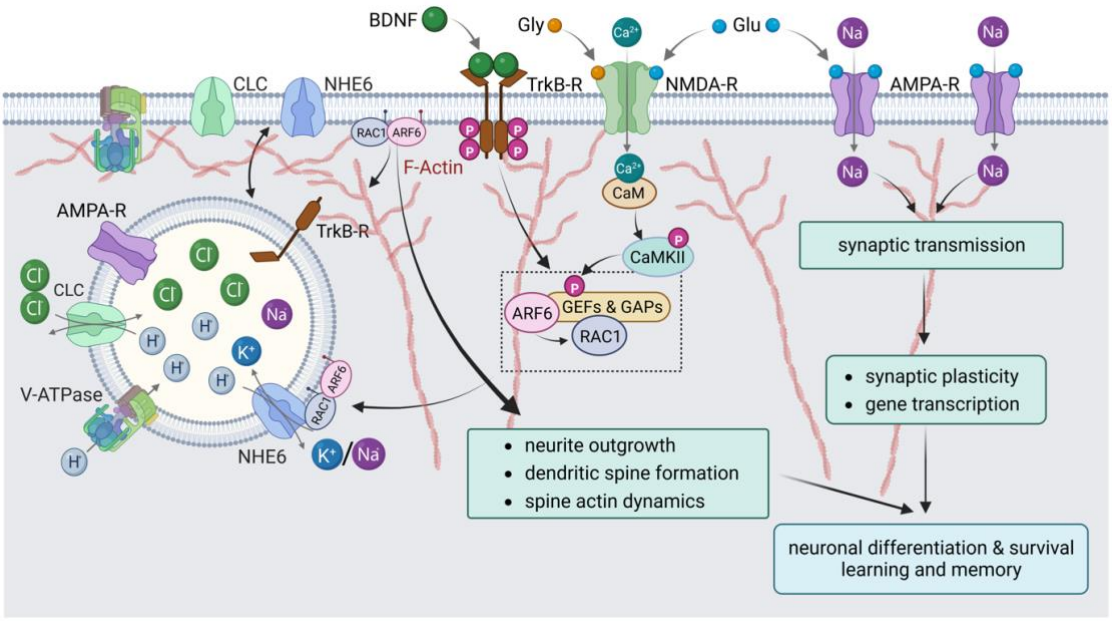

Figure 12 Proposed mechanism of NHE6-positive recycling endosomes carrying RAC1 to and from the cell plasma membrane
Image created with BioRender.

REFERENCES

1. Cohen S, Valm AM, Lippincott-Schwartz J. Interacting Organelles. Curr Opin Cell Biol. 2018 Aug;53:84–91.

2. Scott CC, Gruenberg J. Ion flux and the function of endosomes and lysosomes: pH is just the start. BioEssays. 2011;33(2):103–10.

3. Hu YB, Dammer EB, Ren RJ, Wang G. The endosomal-lysosomal system: from acidification and cargo sorting to neurodegeneration. Transl Neurodegener. 2015 Sep 30;4:18.

4. Casey JR, Grinstein S, Orlowski J. Sensors and regulators of intracellular pH. Nat Rev Mol Cell Biol. 2010 Jan;11(1):50–61.

5. Clague MJ, Urbé S, Aniento F, Gruenberg J. Vacuolar ATPase activity is required for endosomal carrier vesicle formation. Journal of Biological Chemistry. 1994 Jan 7;269(1):21–4.

6. Thattai M. Organelle acidification: an ancient cellular leak detector. BMC Biol. 2017 Jun 26;15:51.

7. Shen J, Zeng Y, Zhuang X, Sun L, Yao X, Pimpl P, et al. Organelle pH in the Arabidopsis Endomembrane System. Molecular Plant. 2013 Sep 1;6(5):1419–37.

8. Diering G, Numata M. Endosomal pH in neuronal signaling and synaptic transmission: role of Na+/H+ exchanger NHE5. Frontiers in Physiology [Internet]. 2014 [cited 2023 Apr 1];4. Available from: https://www.frontiersin.org/articles/10.3389/fphys.2013.00412

9. Forgac M. Vacuolar ATPases: rotary proton pumps in physiology and pathophysiology. Nat Rev Mol Cell Biol. 2007 Nov;8(11):917–29.

10. Grabe M, Oster G. Regulation of Organelle Acidity. J Gen Physiol. 2001 Apr 1;117(4):329–44.

11. Jentsch TJ, Stein V, Weinreich F, Zdebik AA. Molecular Structure and Physiological Function of Chloride Channels. Physiological Reviews. 2002 Apr;82(2):503–68.

12. Poroca DR, Pelis RM, Chappe VM. ClC Channels and Transporters: Structure, Physiological Functions, and Implications in Human Chloride Channelopathies. Frontiers in Pharmacology [Internet]. 2017 [cited 2023 Jun 13];8. Available from: https://www.frontiersin.org/articles/10.3389/fphar.2017.00151

13. Osei-Owusu J, Yang J, Leung KH, Ruan Z, Lü W, Krishnan Y, et al. Proton-activated chloride channel PAC regulates endosomal acidification and transferrin receptor-mediated endocytosis. Cell Rep. 2021 Jan 26;34(4):108683.

14. Freeman SA, Grinstein S, Orlowski J. Determinants, maintenance, and function of organellar pH. Physiol Rev. 2023 Jan 1;103(1):515–606.

15. Ferguson GP, Nikolaev Y, McLaggan D, Maclean M, Booth IR. Survival during exposure to the electrophilic reagent N-ethylmaleimide in Escherichia coli: role of KefB and KefC potassium channels. J Bacteriol. 1997 Feb;179(4):1007–12.

16. Tsujii M, Tanudjaja E, Uozumi N. Diverse Physiological Functions of Cation Proton Antiporters across Bacteria and Plant Cells. Int J Mol Sci. 2020 Jun 26;21(12):4566.

17. Ohsumi Y, Anraku Y. Calcium transport driven by a proton motive force in vacuolar membrane vesicles of Saccharomyces cerevisiae. J Biol Chem. 1983 May 10;258(9):5614–7.

18. Vicogne D, Beauval N, Durin Z, Allorge D, Kondratska K, Haustrate A, et al. Insights into the regulation of cellular Mn2+ homeostasis via TMEM165. Biochimica et Biophysica Acta (BBA) - Molecular Basis of Disease. 2023 Aug 1;1869(6):166717.

19. Demaegd D, Foulquier F, Colinet AS, Gremillon L, Legrand D, Mariot P, et al. Newly characterized Golgi-localized family of proteins is involved in calcium and pH homeostasis in yeast and human cells. Proc Natl Acad Sci U S A. 2013 Apr 23;110(17):6859–64.

20. Reinhardt TA, Lippolis JD, Sacco RE. The Ca2+/H+ antiporter TMEM165 expression, localization in the developing, lactating and involuting mammary gland parallels the secretory pathway Ca2+ ATPase (SPCA1). Biochemical and Biophysical Research Communications. 2014 Mar 7;445(2):417–21.

21. Wang H, Yang Y, Huang F, He Z, Li P, Zhang W, et al. In Situ Fluorescent and Photoacoustic Imaging of Golgi pH to Elucidate the Function of Transmembrane Protein 165. Anal Chem. 2020 Feb 18;92(4):3103–10.

22. Shaul O, Hilgemann DW, de-Almeida-Engler J, Van Montagu M, Inz D, Galili G. Cloning and characterization of a novel Mg(2+)/H(+) exchanger. EMBO J. 1999 Jul 15;18(14):3973–80.

23. Tebar F, Enrich C, Rentero C, Grewal T. GTPases Rac1 and Ras Signaling from Endosomes. Prog Mol Subcell Biol. 2018;57:65–105.

24. Kaksonen M, Roux A. Mechanisms of clathrin-mediated endocytosis. Nat Rev Mol Cell Biol. 2018 May;19(5):313–26.

25. Mayle KM, Le AM, Kamei DT. The Intracellular Trafficking Pathway of Transferrin. Biochim Biophys Acta. 2012 Mar;1820(3):264–81.

26. Klumperman J, Raposo G. The Complex Ultrastructure of the Endolysosomal System. Cold Spring Harb Perspect Biol. 2014 Oct;6(10):a016857.

27. Yamashiro DJ, Maxfield FR. Acidification of endocytic compartments and the intracellular pathways of ligands and receptors. Journal of Cellular Biochemistry. 1984;26(4):231–46.

28. Crichton RR, Charloteaux-Wauters M. Iron transport and storage. European Journal of Biochemistry. 1987;164(3):485–506.

29. Giannetti AM, Snow PM, Zak O, Björkman PJ. Mechanism for Multiple Ligand Recognition by the Human Transferrin Receptor. PLoS Biol. 2003 Dec;1(3):e51.

30. Hurtado-Lorenzo A, Skinner M, Annan JE, Futai M, Sun-Wada GH, Bourgoin S, et al. V-ATPase interacts with ARNO and Arf6 in early endosomes and regulates the protein degradative pathway. Nat Cell Biol. 2006 Feb;8(2):124–36.

31. César-Razquin A, Snijder B, Frappier-Brinton T, Isserlin R, Gyimesi G, Bai X, et al. A Call for Systematic Research on Solute Carriers. Cell. 2015 Jul 30;162(3):478–87.

32. Orlowski J, Grinstein S. Diversity of the mammalian sodium/proton exchanger SLC9 gene family. Pflugers Arch. 2004 Feb;447(5):549–65.

33. Donowitz M, Tse CM, Fuster D. SLC9/NHE gene family, a plasma membrane and organellar family of Na+/H+ exchangers. Mol Aspects Med. 2013;34(0):236–51.

34. Flessner R, Orlowski J. Na+/H+ Exchangers. In: Offermanns S, Rosenthal W, editors. Encyclopedia of Molecular Pharmacology [Internet]. Cham: Springer International Publishing; 2021 [cited 2023 Apr 1]. p. 1047–62. Available from: https://doi.org/10.1007/978-3-030-57401-7_193

35. Padan E, Landau M. Sodium-Proton (Na(+)/H(+)) Antiporters: Properties and Roles in Health and Disease. Met Ions Life Sci. 2016;16:391–458.

36. Moncoq K, Kemp G, Li X, Fliegel L, Young HS. Dimeric Structure of Human Na+/H+ Exchanger Isoform 1 Overproduced in Saccharomyces cerevisiae*. Journal of Biological Chemistry. 2008 Feb 15;283(7):4145–54.

37. Meima ME, Mackley JR, Barber DL. Beyond ion translocation: structural functions of the sodium–hydrogen exchanger isoform-1. Current Opinion in Nephrology and Hypertension. 2007 Jul;16(4):365.

38. Dong Y, Gao Y, Ilie A, Kim D, Boucher A, Li B, et al. Structure and mechanism of the human NHE1-CHP1 complex. Nat Commun. 2021 Jun 9;12(1):3474.

39. Dong Y, Li H, Ilie A, Gao Y, Boucher A, Zhang XC, et al. Structural basis of autoinhibition of the human NHE3-CHP1 complex. Sci Adv. 2022 May 27;8(21):eabn3925.

40. Orlowski J, Grinstein S. Diversity of the mammalian sodium/proton exchanger SLC9 gene family. Pflugers Arch. 2004 Feb;447(5):549–65.

41. Windler F, Bönigk W, Körschen HG, Grahn E, Strünker T, Seifert R, et al. The solute carrier SLC9C1 is a Na+/H+-exchanger gated by an S4-type voltage-sensor and cyclic-nucleotide binding. Nat Commun. 2018 Jul 18;9(1):2809.

42. Fuster DG, Alexander RT. Traditional and emerging roles for the SLC9 Na+/H+ exchangers. Pflugers Arch - Eur J Physiol. 2014 Jan 1;466(1):61–76.

43. Prasad H, Rao R. The Na+/H+ Exchanger NHE6 Modulates Endosomal pH to Control Processing of Amyloid Precursor Protein in a Cell Culture Model of Alzheimer Disease. J Biol Chem. 2015 Feb 27;290(9):5311–27.

44. Ilie A, Boucher A, Park J, Berghuis AM, McKinney RA, Orlowski J. Assorted dysfunctions of endosomal alkali cation/proton exchanger SLC9A6 variants linked to Christianson syndrome. J Biol Chem. 2020 May 15;295(20):7075–95.

45. Zhao H, Carney KE, Falgoust L, Pan JW, Sun D, Zhang Z. Emerging roles of Na+/H+ exchangers in epilepsy and developmental brain disorders. Progress in Neurobiology. 2016 Mar 1;138–140:19–35.

46. Kondapalli KC, Prasad H, Rao R. An inside job: how endosomal Na+/H+ exchangers link to autism and neurological disease. Front Cell Neurosci. 2014 Jun 23;8:172.

47. SLC9A6 solute carrier family 9 member A6 [Homo sapiens (human)] - Gene - NCBI [Internet]. [cited 2023 Apr 1]. Available from: https://www.ncbi.nlm.nih.gov/gene/10479

48. Pescosolido MF, Stein DM, Schmidt M, Achkar CME, Sabbagh M, Rogg JM, et al. Genetic and phenotypic diversity of NHE6 mutations in Christianson syndrome. Ann Neurol. 2014 Oct;76(4):581–93.

49. Morrow EM, Pescosolido MF. Christianson Syndrome. In: Adam MP, Mirzaa GM, Pagon RA, Wallace SE, Bean LJ, Gripp KW, et al., editors. GeneReviews® [Internet]. Seattle (WA): University of Washington, Seattle; 1993 [cited 2023 Apr 1]. Available from: http://www.ncbi.nlm.nih.gov/books/NBK475801/

50. Ouyang Q, Lizarraga SB, Schmidt M, Yang U, Gong J, Ellisor D, et al. Christianson syndrome protein NHE6 modulates TrkB endosomal signaling required for neuronal circuit development. Neuron. 2013 Oct 2;80(1):10.1016/j.neuron.2013.07.043.

51. Gao AYL, Ilie A, Chang PKY, Orlowski J, McKinney RA. A Christianson syndrome-linked deletion mutation (Δ287ES288) in SLC9A6 impairs hippocampal neuronal plasticity. Neurobiology of Disease. 2019 Oct 1;130:104490.

52. Fernandez MA, Bah F, Ma L, Lee Y, Schmidt M, Welch E, et al. Loss of endosomal exchanger NHE6 leads to pathological changes in tau in human neurons. Stem Cell Reports. 2022 Sep 13;17(9):2111–26.

53. Lee Y, Miller MR, Fernandez MA, Berg EL, Prada AM, Ouyang Q, et al. Early lysosome defects precede neurodegeneration with amyloid-β and tau aggregation in NHE6-null rat brain. Brain. 2022 Sep 1;145(9):3187–202.

54. SLC9A7 solute carrier family 9 member A7 [Homo sapiens (human)] - Gene - NCBI [Internet]. [cited 2023 Jul 6]. Available from: https://www.ncbi.nlm.nih.gov/gene?Db=gene&Cmd=DetailsSearch&Term=84679

55. Numata M, Orlowski J. Molecular Cloning and Characterization of a Novel (Na+,K+)/H+ Exchanger Localized to the trans-Golgi Network *. Journal of Biological Chemistry. 2001 May 18;276(20):17387–94.

56. Lin PJC, Williams WP, Luu Y, Molday RS, Orlowski J, Numata M. Secretory carrier membrane proteins interact and regulate trafficking of the organellar (Na+,K+)/H+ exchanger NHE7. J Cell Sci. 2005 May 1;118(Pt 9):1885–97.

57. Khayat W, Hackett A, Shaw M, Ilie A, Dudding-Byth T, Kalscheuer VM, et al. A recurrent missense variant in SLC9A7 causes nonsyndromic X-linked intellectual disability with alteration of Golgi acidification and aberrant glycosylation. Human Molecular Genetics. 2019 Feb 15;28(4):598–614.

58. Goyal S, Vanden Heuvel G, Aronson PS. Renal expression of novel Na+/H+ exchanger isoform NHE8. Am J Physiol Renal Physiol. 2003 Mar;284(3):F467-473.

59. Xu H, Zhang B, Li J, Chen H, Tooley J, Ghishan FK. Epidermal growth factor inhibits intestinal NHE8 expression via reducing its basal transcription. Am J Physiol Cell Physiol. 2010 Jul;299(1):C51-57.

60. Zhang J, Bobulescu IA, Goyal S, Aronson PS, Baum MG, Moe OW. Characterization of Na+/H+ exchanger NHE8 in cultured renal epithelial cells. American Journal of Physiology-Renal Physiology. 2007 Sep;293(3):F761–6.

61. Goyal S, Mentone S, Aronson PS. Immunolocalization of NHE8 in rat kidney. Am J Physiol Renal Physiol. 2005 Mar;288(3):F530-538.

62. Lawrence SP, Bright NA, Luzio JP, Bowers K. The Sodium/Proton Exchanger NHE8 Regulates Late Endosomal Morphology and Function. Mol Biol Cell. 2010 Oct 15;21(20):3540–51.

63. Bernardazzi C, Xu H, Tong H, Laubitz D, Figliuolo da Paz V, Curiel L, et al. An indisputable role of NHE8 in mucosal protection. American Journal of Physiology-Gastrointestinal and Liver Physiology. 2020 Oct;319(4):G421–31.

64. Xu H, Ghishan FK, Kiela PR. SLC9 Gene Family: Function, Expression, and Regulation. Compr Physiol. 2018 Mar 26;8(2):555–83.

65. de Silva MG, Elliott K, Dahl H, Fitzpatrick E, Wilcox S, Delatycki M, et al. Disruption of a novel member of a sodium/hydrogen exchanger family and DOCK3 is associated with an attention deficit hyperactivity disorder-like phenotype. J Med Genet. 2003 Oct;40(10):733–40.

66. Roxrud I, Raiborg C, Gilfillan GD, Strømme P, Stenmark H. Dual degradation mechanisms ensure disposal of NHE6 mutant protein associated with neurological disease. Exp Cell Res. 2009 Oct 15;315(17):3014–27.

67. PubChem. SLC9A9 - solute carrier family 9 member A9 (human) [Internet]. [cited 2023 Jul 25]. Available from: https://pubchem.ncbi.nlm.nih.gov/gene/SLC9A9/human

68. Schwede M, Garbett K, Mirnics K, Geschwind DH, Morrow EM. Genes for endosomal NHE6 and NHE9 are misregulated in autism brains. Mol Psychiatry. 2014 Mar;19(3):277–9.

69. Markunas CA, Quinn KS, Collins AL, Garrett ME, Lachiewicz AM, Sommer JL, et al. Genetic variants in SLC9A9 are associated with measures of Attention-deficit/hyperactivity disorder symptoms in families. Psychiatr Genet. 2010 Apr;20(2):73–81.

70. Cardon M, Evankovich KD, Holder JL. Exonic deletion of SLC9A9 in autism with epilepsy. Neurol Genet. 2016 Apr;2(2):e62.

71. Christianson A, Stevenson R, van der Meyden CH, Pelser J, Theron F, van Rensburg PL, et al. X linked severe mental retardation, craniofacial dysmorphology, epilepsy, ophthalmoplegia, and cerebellar atrophy in a large South African kindred is localised to Xq24-q27. J Med Genet. 1999 Oct;36(10):759–66.

72. Gilfillan GD, Selmer KK, Roxrud I, Smith R, Kyllerman M, Eiklid K, et al. SLC9A6 mutations cause X-linked mental retardation, microcephaly, epilepsy, and ataxia, a phenotype mimicking Angelman syndrome. Am J Hum Genet. 2008 Apr;82(4):1003–10.

73. Tarpey PS, Smith R, Pleasance E, Whibley A, Edkins S, Hardy C, et al. A systematic, large-scale resequencing screen of X-chromosome coding exons in mental retardation. Nat Genet. 2009 May;41(5):535–43.

74. Neri G, Schwartz CE, Lubs HA, Stevenson RE. XLID Update 2017. Am J Med Genet A. 2018 Jun;176(6):1375–88.

75. Nan H, Kim YJ, Tsuchiya M, Ishida A, Haro H, Hiraide M, et al. Novel SLC9A6 Variation in Female Carriers With Intellectual Disability and Atypical Parkinsonism. Neurol Genet. 2022 Feb;8(1):e651.

76. Pescosolido MF, Kavanaugh BC, Pochet N, Schmidt M, Jerskey BA, Rogg JM, et al. Complex Neurological Phenotype in Female Carriers of NHE6 Mutations. Mol Neuropsychiatry. 2019 Apr;5(2):98–108.

77. Sikora J, Leddy J, Gulinello M, Walkley SU. X-linked Christianson syndrome: heterozygous female Slc9a6 knockout mice develop mosaic neuropathological changes and related behavioral abnormalities. Dis Model Mech. 2016 Jan 1;9(1):13–23.

78. Garbern JY, Neumann M, Trojanowski JQ, Lee VMY, Feldman G, Norris JW, et al. A mutation affecting the sodium/proton exchanger, SLC9A6, causes mental retardation with tau deposition. Brain. 2010 May;133(5):1391–402.

79. Dagli AI, Mathews J, Williams CA. Angelman Syndrome. In: Adam MP, Mirzaa GM, Pagon RA, Wallace SE, Bean LJ, Gripp KW, et al., editors. GeneReviews® [Internet]. Seattle (WA): University of Washington, Seattle; 1993 [cited 2023 Jul 4]. Available from: http://www.ncbi.nlm.nih.gov/books/NBK1144/

80. Moser MB, Moser EI. Functional differentiation in the hippocampus. Hippocampus. 1998;8(6):608–19.

81. Deane EC, Ilie AE, Sizdahkhani S, Gupta MD, Orlowski J, McKinney RA. Enhanced Recruitment of Endosomal Na+/H+ Exchanger NHE6 into Dendritic Spines of Hippocampal Pyramidal Neurons during NMDA Receptor-Dependent Long-Term Potentiation. J Neurosci. 2013 Jan 9;33(2):595–610.

82. Xinhan L, Matsushita M, Numaza M, Taguchi A, Mitsui K, Kanazawa H. Na+/H+ exchanger isoform 6 (NHE6/SLC9A6) is involved in clathrin-dependent endocytosis of transferrin. Am J Physiol Cell Physiol. 2011 Dec;301(6):C1431-1444.

83. Lüscher C, Malenka RC. NMDA Receptor-Dependent Long-Term Potentiation and Long-Term Depression (LTP/LTD). Cold Spring Harb Perspect Biol. 2012 Jun;4(6):a005710.

84. Chao MV, Lee FS. Neurotrophin survival signaling mechanisms. J Alzheimers Dis. 2004 Dec;6(6 Suppl):S7-11.

85. Danzer SC, Crooks KRC, Lo DC, McNamara JO. Increased Expression of Brain-Derived Neurotrophic Factor Induces Formation of Basal Dendrites and Axonal Branching in Dentate Granule Cells in Hippocampal Explant Cultures. J Neurosci. 2002 Nov 15;22(22):9754–63.

86. Petitjean H, Fatima T, Mouchbahani-Constance S, Davidova A, Ferland CE, Orlowski J, et al. Loss of SLC9A6/NHE6 impairs nociception in a mouse model of Christianson syndrome. Pain. 2020 Nov;161(11):2619–28.

87. Figueroa KP, Anderson CJ, Paul S, Dansithong W, Gandelman M, Scoles DR, et al. Slc9a6 mutation causes Purkinje cell loss and ataxia in the shaker rat. Hum Mol Genet. 2023 Jan 9;ddad004.

88. Ilie A, Gao AYL, Boucher A, Park J, Berghuis AM, Hoffer MJV, et al. A potential gain-of-function variant of SLC9A6 leads to endosomal alkalinization and neuronal atrophy associated with Christianson Syndrome. Neurobiol Dis. 2019 Jan;121:187–204.

89. Brückner A, Polge C, Lentze N, Auerbach D, Schlattner U. Yeast Two-Hybrid, a Powerful Tool for Systems Biology. Int J Mol Sci. 2009 Jun 18;10(6):2763–88.

90. Roux KJ, Kim DI, Burke B, May DG. BioID: A Screen for Protein-Protein Interactions. Curr Protoc Protein Sci. 2018 Feb 21;91:19.23.1-19.23.15.

91. Roux KJ, Kim DI, Raida M, Burke B. A promiscuous biotin ligase fusion protein identifies proximal and interacting proteins in mammalian cells. Journal of Cell Biology. 2012 Mar 12;196(6):801–10.

92. Cho KF, Branon TC, Udeshi ND, Myers SA, Carr SA, Ting AY. Proximity labeling in mammalian cells with TurboID and split-TurboID. Nat Protoc. 2020 Dec;15(12):3971–99.

93. Branon TC, Bosch JA, Sanchez AD, Udeshi ND, Svinkina T, Carr SA, et al. Efficient proximity labeling in living cells and organisms with TurboID. Nat Biotechnol. 2018 Oct;36(9):880–7.

94. Kalocsay M. APEX Peroxidase-Catalyzed Proximity Labeling and Multiplexed Quantitative Proteomics. Methods Mol Biol. 2019;2008:41–55.

95. Santos-Barriopedro I, van Mierlo G, Vermeulen M. Off-the-shelf proximity biotinylation for interaction proteomics. Nat Commun. 2021 Aug 18;12(1):5015.

96. Ilie A, Gao AYL, Reid J, Boucher A, McEwan C, Barrière H, et al. A Christianson syndrome-linked deletion mutation (Δ(287)ES(288)) in SLC9A6 disrupts recycling endosomal function and elicits neurodegeneration and cell death. Mol Neurodegener. 2016 Sep 2;11(1):63.

97. Hung V, Udeshi ND, Lam SS, Loh KH, Cox KJ, Pedram K, et al. Spatially resolved proteomic mapping in living cells with the engineered peroxidase APEX2. Nat Protoc. 2016 Mar;11(3):456–75.

98. Rhee HW, Zou P, Udeshi ND, Martell JD, Mootha VK, Carr SA, et al. Proteomic Mapping of Mitochondria in Living Cells via Spatially-Restricted Enzymatic Tagging. Science. 2013 Mar 15;339(6125):1328–31.

99. Hung V, Zou P, Rhee HW, Udeshi ND, Cracan V, Svinkina T, et al. Proteomic mapping of the human mitochondrial intermembrane space in live cells via ratiometric APEX tagging. Mol Cell. 2014 Jul 17;55(2):332–41.

100. Martell JD, Deerinck TJ, Lam SS, Ellisman MH, Ting AY. Electron microscopy using the genetically encoded APEX2 tag in cultured mammalian cells. Nat Protoc. 2017 Sep;12(9):1792–816.

101. Rotin D, Grinstein S. Impaired cell volume regulation in Na(+)-H+ exchange-deficient mutants. Am J Physiol. 1989 Dec;257(6 Pt 1):C1158-1165.

102. Wilson JM, Colton TL. Targeting of an Intestinal Apical Endosomal Protein to Endosomes in Nonpolarized Cells. J Cell Biol. 1997 Jan 27;136(2):319–30.

103. Coorssen JR, Schmitt H, Almers W. Ca2+ triggers massive exocytosis in Chinese hamster ovary cells. EMBO J. 1996 Aug 1;15(15):3787–91.

104. Zhang T, Gygi SP, Paulo JA. Temporal Proteomic Profiling of SH-SY5Y Differentiation with Retinoic Acid Using FAIMS and Real-Time Searching. J Proteome Res. 2021 Jan 1;20(1):704–14.

105. Li J, Ma Z, Shi M, Malty RH, Aoki H, Minic Z, et al. Identification of Human Neuronal Protein Complexes Reveals Biochemical Activities and Convergent Mechanisms of Action in Autism Spectrum Disorders. Cell Systems. 2015 Nov 25;1(5):361–74.

106. Kovalevich J, Langford D. Considerations for the Use of SH-SY5Y Neuroblastoma Cells in Neurobiology. Methods Mol Biol. 2013;1078:9–21.

107. Hodge K, Have ST, Hutton L, Lamond AI. Cleaning up the masses: Exclusion lists to reduce contamination with HPLC-MS/MS. J Proteomics. 2013 Aug 2;88:92–103.

108. Keller BO, Sui J, Young AB, Whittal RM. Interferences and contaminants encountered in modern mass spectrometry. Analytica Chimica Acta. 2008 Oct 3;627(1):71–81.

109. Niers JM, Chen JW, Weissleder R, Tannous BA. Enhanced in vivo imaging of metabolically biotinylated cell surface reporters. Anal Chem. 2011 Feb 1;83(3):994–9.

110. Ge SX, Jung D, Yao R. ShinyGO: a graphical gene-set enrichment tool for animals and plants. Bioinformatics. 2020 Apr 15;36(8):2628–9.

111. Szklarczyk D, Gable AL, Nastou KC, Lyon D, Kirsch R, Pyysalo S, et al. The STRING database in 2021: customizable protein-protein networks, and functional characterization of user-uploaded gene/measurement sets. Nucleic Acids Res. 2021 Jan 8;49(D1):D605–12.

112. STRING: functional protein association networks [Internet]. [cited 2023 Apr 4]. Available from: https://string-db.org/cgi/input?sessionId=bOsvxPsGbuyC&input_page_show_search=on

113. Kanehisa M, Goto S. KEGG: kyoto encyclopedia of genes and genomes. Nucleic Acids Res. 2000 Jan 1;28(1):27–30.

114. Borovac J, Bosch M, Okamoto K. Regulation of actin dynamics during structural plasticity of dendritic spines: Signaling messengers and actin-binding proteins. Mol Cell Neurosci. 2018 Sep;91:122–30.

115. Hering H, Sheng M. Activity-dependent redistribution and essential role of cortactin in dendritic spine morphogenesis. J Neurosci. 2003 Dec 17;23(37):11759–69.

116. Huang Z, Shimazu K, Woo NH, Zang K, Müller U, Lu B, et al. Distinct roles of the beta 1-class integrins at the developing and the mature hippocampal excitatory synapse. J Neurosci. 2006 Oct 25;26(43):11208–19.

117. Kawauchi T, Hoshino M. Molecular pathways regulating cytoskeletal organization and morphological changes in migrating neurons. Dev Neurosci. 2008;30(1–3):36–46.

118. Sydor AM, Su AL, Wang FS, Xu A, Jay DG. Talin and vinculin play distinct roles in filopodial motility in the neuronal growth cone. J Cell Biol. 1996 Sep;134(5):1197–207.

119. Luo S, Schaefer AM, Dour S, Nonet ML. The conserved LIM domain-containing focal adhesion protein ZYX-1 regulates synapse maintenance in Caenorhabditis elegans. Development. 2014 Oct;141(20):3922–33.

120. Hanyaloglu AC, McCullagh E, von Zastrow M. Essential role of Hrs in a recycling mechanism mediating functional resensitization of cell signaling. EMBO J. 2005 Jul 6;24(13):2265–83.

121. Zhang G, Deinhardt K, Chao MV, Neubert TA. Study of neurotrophin-3 signaling in primary cultured neurons using multiplex stable isotope labeling with amino acids in cell culture. J Proteome Res. 2011 May 6;10(5):2546–54.

122. Lee U, Choi C, Ryu SH, Park D, Lee SE, Kim K, et al. SCAMP5 plays a critical role in axonal trafficking and synaptic localization of NHE6 to adjust quantal size at glutamatergic synapses. Proc Natl Acad Sci U S A. 2021 Jan 12;118(2):e2011371118.

123. Cai Q, Pan PY, Sheng ZH. Syntabulin-kinesin-1 family member 5B-mediated axonal transport contributes to activity-dependent presynaptic assembly. J Neurosci. 2007 Jul 4;27(27):7284–96.

124. Rivera J, Chu PJ, Lewis TL, Arnold DB. The role of Kif5B in axonal localization of Kv1 K(+) channels. Eur J Neurosci. 2007 Jan;25(1):136–46.

125. Zhao J, Fok AHK, Fan R, Kwan PY, Chan HL, Lo LHY, et al. Specific depletion of the motor protein KIF5B leads to deficits in dendritic transport, synaptic plasticity and memory. Kim E, Cooper JA, Bao L, editors. eLife. 2020 Jan 21;9:e53456.

126. Schiavo G, Greensmith L, Hafezparast M, Fisher EMC. Cytoplasmic dynein heavy chain: the servant of many masters. Trends Neurosci. 2013 Nov;36(11):641–51.

127. Willemsen MH, Vissers LEL, Willemsen MAAP, van Bon BWM, Kroes T, de Ligt J, et al. Mutations in DYNC1H1 cause severe intellectual disability with neuronal migration defects. J Med Genet. 2012 Mar;49(3):179–83.

128. Garrett CA, Barri M, Kuta A, Soura V, Deng W, Fisher EMC, et al. DYNC1H1 mutation alters transport kinetics and ERK1/2-cFos signalling in a mouse model of distal spinal muscular atrophy. Brain. 2014 Jul;137(Pt 7):1883–93.

129. Peeters K, Bervoets S, Chamova T, Litvinenko I, De Vriendt E, Bichev S, et al. Novel mutations in the DYNC1H1 tail domain refine the genetic and clinical spectrum of dyneinopathies. Hum Mutat. 2015 Mar;36(3):287–91.

130. Schrötter A, Oberhaus A, Kolbe K, Seger S, Mastalski T, El Magraoui F, et al. LMD proteomics provides evidence for hippocampus field-specific motor protein abundance changes with relevance to Alzheimer's disease. Biochim Biophys Acta Proteins Proteom. 2017 Jun;1865(6):703–14.

131. Matsumoto A, Kojima K, Miya F, Miyauchi A, Watanabe K, Iwamoto S, et al. Two cases of DYNC1H1 mutations with intractable epilepsy. Brain Dev. 2021 Sep;43(8):857–62.

132. Thurston CF, Henley LF. Direct immunoprecipitation of protein. Methods Mol Biol. 1988;3:149–58.

133. Lin JS, Lai EM. Protein-Protein Interactions: Co-Immunoprecipitation. Methods Mol Biol. 2017;1615:211–9.

134. Phizicky EM, Fields S. Protein-protein interactions: methods for detection and analysis. Microbiol Rev. 1995 Mar;59(1):94–123.

135. Bosco EE, Mulloy JC, Zheng Y. Rac1 GTPase: a "Rac" of all trades. Cell Mol Life Sci. 2009 Feb;66(3):370–4.

136. Majolée J, Podieh F, Hordijk PL, Kovačević I. The interplay of Rac1 activity, ubiquitination and GDI binding and its consequences for endothelial cell spreading. PLoS One. 2021 Jul 12;16(7):e0254386.

137. Wong KW, Mohammadi S, Isberg RR. Disruption of RhoGDI and RhoA Regulation by a Rac1 Specificity Switch Mutant*. Journal of Biological Chemistry. 2006 Dec 29;281(52):40379–88.

138. Sambrook J, Russell DW. Detection of Protein-Protein Interactions Using the GST Fusion Protein Pulldown Technique. CSH Protoc. 2006 Jun 1;2006(1):pdb.prot3757.

139. Kim SY, Hakoshima T. GST Pull-Down Assay to Measure Complex Formations. Methods Mol Biol. 2019;1893:273–80.

140. Ilie A, Weinstein E, Boucher A, McKinney RA, Orlowski J. Impaired posttranslational processing and trafficking of an endosomal Na+/H+ exchanger NHE6 mutant (Δ(370)WST(372)) associated with X-linked intellectual disability and autism. Neurochem Int. 2014 Jul;73:192–203.

141. Bouchet J, Del Río-Iñiguez I, Lasserre R, Agüera-Gonzalez S, Cuche C, Danckaert A, et al. Rac1-Rab11-FIP3 regulatory hub coordinates vesicle traffic with actin remodeling and T-cell activation. EMBO J. 2016 Jun 1;35(11):1160–74.

142. Stanley AC, Wong CX, Micaroni M, Venturato J, Khromykh T, Stow JL, et al. The Rho GTPase Rac1 is required for recycling endosome-mediated secretion of TNF in macrophages. Immunol Cell Biol. 2014 Mar;92(3):275–86.

143. Michaelson D, Silletti J, Murphy G, D'Eustachio P, Rush M, Philips MR. Differential localization of Rho GTPases in live cells: regulation by hypervariable regions and RhoGDI binding. J Cell Biol. 2001 Jan 8;152(1):111–26.

144. Dransart E, Morin A, Cherfils J, Olofsson B. Uncoupling of Inhibitory and Shuttling Functions of Rho GDP Dissociation Inhibitors*. Journal of Biological Chemistry. 2005 Feb 11;280(6):4674–83.

145. Lamaze C, Chuang TH, Terlecky LJ, Bokoch GM, Schmid SL. Regulation of receptor-mediated endocytosis by Rho and Rac. Nature. 1996 Jul 11;382(6587):177–9.

146. Prieto-Sánchez RM, Bustelo XR. Structural Basis for the Signaling Specificity of RhoG and Rac1 GTPases*. Journal of Biological Chemistry. 2003 Sep 26;278(39):37916–25.

147. Ohgaki R, Matsushita M, Kanazawa H, Ogihara S, Hoekstra D, van IJzendoorn SCD. The Na+/H+ Exchanger NHE6 in the Endosomal Recycling System Is Involved in the Development of Apical Bile Canalicular Surface Domains in HepG2 Cells. Mol Biol Cell. 2010 Apr 1;21(7):1293–304.

148. Kraynov VS, Chamberlain C, Bokoch GM, Schwartz MA, Slabaugh S, Hahn KM. Localized Rac activation dynamics visualized in living cells. Science. 2000 Oct 13;290(5490):333–7.

149. Pischedda F, Szczurkowska J, Cirnaru MD, Giesert F, Vezzoli E, Ueffing M, et al. A Cell Surface Biotinylation Assay to Reveal Membrane-associated Neuronal Cues: Negr1 Regulates Dendritic Arborization. Mol Cell Proteomics. 2014 Mar;13(3):733–48.

150. Mirsaeidi M, Gidfar S, Vu A, Schraufnagel D. Annexins family: insights into their functions and potential role in pathogenesis of sarcoidosis. Journal of Translational Medicine. 2016 Apr 12;14(1):89.

151. Moss SE, Morgan RO. The annexins. Genome Biol. 2004;5(4):219.

152. Wong CO. Endosomal-Lysosomal Processing of Neurodegeneration-Associated Proteins in Astrocytes. Int J Mol Sci. 2020 Jul 21;21(14):5149.

153. Nakamura F, Stossel TP, Hartwig JH. The filamins. Cell Adh Migr. 2011;5(2):160–9.

154. Lee G, Schwarz TL. Filamin, a synaptic organizer in Drosophila, determines glutamate receptor composition and membrane growth. eLife. 5:e19991.

155. Uruno T, Liu J, Zhang P, Fan Yx null, Egile C, Li R, et al. Activation of Arp2/3 complex-mediated actin polymerization by cortactin. Nat Cell Biol. 2001 Mar;3(3):259–66.

156. Weaver AM, Karginov AV, Kinley AW, Weed SA, Li Y, Parsons JT, et al. Cortactin promotes and stabilizes Arp2/3-induced actin filament network formation. Curr Biol. 2001 Mar 6;11(5):370–4.

157. Lin JJ, Li Y, Eppinga RD, Wang Q, Jin J. Chapter 1 Roles of Caldesmon in Cell Motility and Actin Cytoskeleton Remodeling. In: International Review of Cell and Molecular Biology [Internet]. Academic Press; 2009 [cited 2023 Jul 30]. p. 1–68. (International Review of Cell and Molecular Biology; vol. 274). Available from: https://www.sciencedirect.com/science/article/pii/S1937644808020017

158. Huang R, Cao GJ, Guo H, Kordowska J, Wang CLA. Direct Interaction between Caldesmon and Cortactin. Arch Biochem Biophys. 2006 Dec 15;456(2):175–82.

159. Mohan R, John A. Microtubule-associated proteins as direct crosslinkers of actin filaments and microtubules. IUBMB Life. 2015;67(6):395–403.

160. Riederer BM. Microtubule-associated protein 1B, a growth-associated and phosphorylated scaffold protein. Brain Research Bulletin. 2007 Mar 30;71(6):541–58.

161. Zervas M, Opitz T, Edelmann W, Wainer B, Kucherlapati R, Stanton PK. Impaired hippocampal long-term potentiation in microtubule-associated protein 1B-deficient mice. Journal of Neuroscience Research. 2005;82(1):83–92.

162. Tokuraku K, Okuyama S, Matsushima K, Ikezu T, Kotani S. Distinct neuronal localization of microtubule-associated protein 4 in the mammalian brain. Neuroscience Letters. 2010 Oct 29;484(2):143–7.

163. Nakayama AY, Harms MB, Luo L. Small GTPases Rac and Rho in the Maintenance of Dendritic Spines and Branches in Hippocampal Pyramidal Neurons. J Neurosci. 2000 Jul 15;20(14):5329–38.

164. Etienne-Manneville S, Hall A. Rho GTPases in cell biology. Nature. 2002 Dec 12;420(6916):629–35.

165. Sugihara K, Nakatsuji N, Nakamura K, Nakao K, Hashimoto R, Otani H, et al. Rac1 is required for the formation of three germ layers during gastrulation. Oncogene. 1998 Dec;17(26):3427–33.

166. Hua ZL, Emiliani FE, Nathans J. Rac1 plays an essential role in axon growth and guidance and in neuronal survival in the central and peripheral nervous systems. Neural Development. 2015 Sep 23;10(1):21.

167. Murakoshi H, Wang H, Yasuda R. Local, persistent activation of Rho GTPases during plasticity of single dendritic spines. Nature. 2011 Apr 7;472(7341):100–4.

168. Diering GH, Mills F, Bamji SX, Numata M. Regulation of dendritic spine growth through activity-dependent recruitment of the brain-enriched Na+/H+ exchanger NHE5. Mol Biol Cell. 2011 Jul 1;22(13):2246–57.

169. Bongmba OYN, Martinez LA, Elhardt ME, Butler K, Tejada-Simon MV. Modulation of dendritic spines and synaptic function by Rac1: A possible link to Fragile X syndrome pathology. Brain Res. 2011 Jul 5;1399:79–95.

170. Chung CY, Lee S, Briscoe C, Ellsworth C, Firtel RA. Role of Rac in controlling the actin cytoskeleton and chemotaxis in motile cells. Proc Natl Acad Sci U S A. 2000 May 9;97(10):5225–30.

171. Allen WE, Zicha D, Ridley AJ, Jones GE. A Role for Cdc42 in Macrophage Chemotaxis. J Cell Biol. 1998 Jun 1;141(5):1147–57.

172. De P, Aske JC, Dey N. RAC1 Takes the Lead in Solid Tumors. Cells. 2019 Apr 26;8(5):382.

173. Liang J, Oyang L, Rao S, Han Y, Luo X, Yi P, et al. Rac1, A Potential Target for Tumor Therapy. Front Oncol. 2021 May 17;11:674426.

174. Das S, Yin T, Yang Q, Zhang J, Wu YI, Yu J. Single-molecule tracking of small GTPase Rac1 uncovers spatial regulation of membrane translocation and mechanism for polarized signaling. Proceedings of the National Academy of Sciences. 2015 Jan 20;112(3):E267–76.

175. Xie Z, Srivastava DP, Photowala H, Kai L, Cahill ME, Woolfrey KM, et al. Kalirin-7 controls activity-dependent structural and functional plasticity of dendritic spines. Neuron. 2007 Nov 22;56(4):640–56.

176. Marei H, Malliri A. GEFs: Dual regulation of Rac1 signaling. Small GTPases. 2016 Jun 17;8(2):90–9.

177. Saneyoshi T, Matsuno H, Suzuki A, Murakoshi H, Hedrick NG, Agnello E, et al. Reciprocal activation within a kinase-effector complex underlying persistence of structural LTP. Neuron. 2019 Jun 19;102(6):1199-1210.e6.

178. Yamauchi T. Neuronal Ca^{2+}/Calmodulin-Dependent Protein Kinase II—Discovery, Progress in a Quarter of a Century, and Perspective: Implication for Learning and Memory. Biological and Pharmaceutical Bulletin. 2005;28(8):1342–54.

179. Pontrello CG, Ethell IM. Accelerators, Brakes, and Gears of Actin Dynamics in Dendritic Spines. Open Neurosci J. 2009 Jan 1;3:67–86.

180. Cingolani LA, Goda Y. Actin in action: the interplay between the actin cytoskeleton and synaptic efficacy. Nat Rev Neurosci. 2008 May;9(5):344–56.

181. Pyronneau A, He Q, Hwang JY, Porch M, Contractor A, Zukin RS. Aberrant Rac1-cofilin signaling mediates defects in dendritic spines, synaptic function, and sensory perception in fragile X syndrome. Sci Signal. 2017 Nov 7;10(504):eaan0852.

182. Bamburg JR, Bernstein BW. Roles of ADF/cofilin in actin polymerization and beyond. F1000 Biol Rep. 2010 Aug 19;2:62.

183. Arber S, Barbayannis FA, Hanser H, Schneider C, Stanyon CA, Bernard O, et al. Regulation of actin dynamics through phosphorylation of cofilin by LIM-kinase. Nature. 1998 Jun 25;393(6687):805–9.

184. Margiotta A, Progida C, Bakke O, Bucci C. Rab7a regulates cell migration through Rac1 and vimentin. Biochimica et Biophysica Acta (BBA) - Molecular Cell Research. 2017 Feb 1;1864(2):367–81.

185. Deinhardt K, Salinas S, Verastegui C, Watson R, Worth D, Hanrahan S, et al. Rab5 and Rab7 Control Endocytic Sorting along the Axonal Retrograde Transport Pathway. Neuron. 2006 Oct 19;52(2):293–305.

186. Bailey CH, Kandel ER. Structural changes accompanying memory storage. Annu Rev Physiol. 1993;55:397–426.

187. Szászi K, Kurashima K, Kapus A, Paulsen A, Kaibuchi K, Grinstein S, et al. RhoA and rho kinase regulate the epithelial Na+/H+ exchanger NHE3. Role of myosin light chain phosphorylation. J Biol Chem. 2000 Sep 15;275(37):28599–606.

188. Chan WWR, Li W, Chang RCC, Lau KF. ARF6-Rac1 signaling-mediated neurite outgrowth is potentiated by the neuronal adaptor FE65 through orchestrating ARF6 and ELMO1. FASEB J. 2020 Dec;34(12):16397–413.

189. Ohgaki R, Fukura N, Matsushita M, Mitsui K, Kanazawa H. Cell Surface Levels of Organellar Na+/H+ Exchanger Isoform 6 Are Regulated by Interaction with RACK1 *. Journal of Biological Chemistry. 2008 Feb 15;283(7):4417–29.

190. Pulakat L, Cooper S, Knowle D, Mandavia C, Bruhl S, Hetrick M, et al. Ligand-dependent complex formation between the Angiotensin II receptor subtype AT2 and Na+/H+ exchanger NHE6 in mammalian cells. Peptides. 2005 May 1;26(5):863–73.

191. Blume A, Kaschina E, Unger T. Angiotensin II type 2 receptors: signalling and pathophysiological role. Curr Opin Nephrol Hypertens. 2001 Mar;10(2):239–46.

192. Libonati JR, Eberli FR, Sesselberg HW, Apstein CS. Effects of low-flow ischemia on the positive inotropic action of angiotensin II in isolated rabbit and rat hearts. Cardiovasc Res. 1997 Jan;33(1):71–81.

193. Ito N, Kagaya Y, Weinberg EO, Barry WH, Lorell BH. Endothelin and angiotensin II stimulation of Na+-H+ exchange is impaired in cardiac hypertrophy. J Clin Invest. 1997 Jan 1;99(1):125–35.

194. Fröhlich O, Karmazyn M. The Na–H exchanger revisited: an update on Na–H exchange regulation and the role of the exchanger in hypertension and cardiac function in health and disease. Cardiovascular Research. 1997 Nov 1;36(2):138–48.